AD-A154 378 STRAIN-PATH MODELING FOR GEO-MATERIALS(U) APPLIED THEORY INC LOS ANGELES CA J G TRULIO 07 MAR 84 ATR-83-65-1 DNA-TR-84-105 DNA001-84-C-0128 1/1

UNCLASSIFIED F/G 8/7 NL

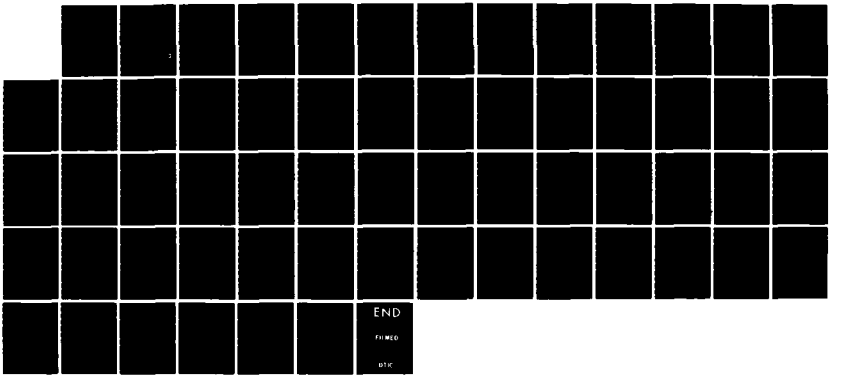

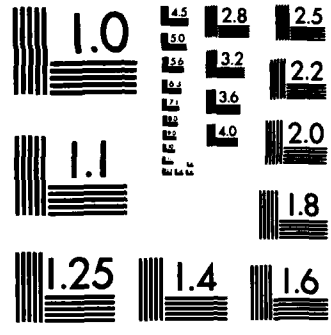

MICROCOPY RESOLUTION TEST CHART
NATIONAL BUREAU OF STANDARDS-1963-A

DNA-TR-84-105

STRAIN-PATH MODELING FOR GEO-MATERIALS

John G. Trulio
Applied Theory, Inc.
930 South La Brea Avenue
Los Angeles, CA 90036-4808

7 March 1984

Technical Report

CONTRACT No. DNA 001-84-C-0128

THIS WORK WAS SPONSORED BY THE DEFENSE NUCLEAR AGENCY
UNDER RDT&E RMSS CODE X341084469 Q93QMXSA00009 H2590D.

Prepared for
Director
DEFENSE NUCLEAR AGENCY
Washington, DC 20305-1000

Destroy this report when it is no longer needed. Do not return to sender.

PLEASE NOTIFY THE DEFENSE NUCLEAR AGENCY, ATTN: STTI, WASHINGTON, DC 20305-1000, IF YOUR ADDRESS IS INCORRECT, IF YOU WISH IT DELETED FROM THE DISTRIBUTION LIST, OR IF THE ADDRESSEE IS NO LONGER EMPLOYED BY YOUR ORGANIZATION.

UNCLASSIFIED

SECURITY CLASSIFICATION OF THIS PAGE (When Data Entered)

REPORT DOCUMENTATION PAGE		READ INSTRUCTIONS BEFORE COMPLETING FORM
1. REPORT NUMBER DNA-TR-84-105	2. GOVT ACCESSION NO. AD-A154378	3. RECIPIENT'S CATALOG NUMBER
4. TITLE (and Subtitle) STRAIN-PATH MODELING FOR GEO-MATERIALS		5. TYPE OF REPORT & PERIOD COVERED Technical Report
		6. PERFORMING ORG. REPORT NUMBER ATR-83-65-1
7. AUTHOR(s) John G. Trulio		8. CONTRACT OR GRANT NUMBER(s) DNA 001-84-C-0128
9. PERFORMING ORGANIZATION NAME AND ADDRESS Applied Theory, Inc. 930 South La Brea Avenue Los Angeles, CA 90036-4808		10. PROGRAM ELEMENT, PROJECT, TASK AREA & WORK UNIT NUMBERS Task Q93QMXSA-00009
11. CONTROLLING OFFICE NAME AND ADDRESS Director Defense Nuclear Agency Washington, DC 20305-1000		12. REPORT DATE 7 March 1984 13. NUMBER OF PAGES 58
14. MONITORING AGENCY NAME & ADDRESS(if different from Controlling Office)		15. SECURITY CLASS (of this report) UNCLASSIFIED 15a. DECLASSIFICATION/DOWNGRADING SCHEDULE N/A since UNCLASSIFIED

16. DISTRIBUTION STATEMENT (of this Report)

Approved for public release; distribution unlimited.

17. DISTRIBUTION STATEMENT (of the abstract entered in Block 20, if different from Report)

18. SUPPLEMENTARY NOTES

This work was sponsored by the Defense Nuclear Agency under RDT&E RMSS Code X341084469 Q93QMXSA00009 H2590D.

19. KEY WORDS (Continue on reverse side if necessary and identify by block number)

Geologic Media	In-Situ Measurements
Stress Measurements	Physical Properties
Hydrostatic Tests	Mechanical Properties
Ground Shock Waves	

20. ABSTRACT (Continue on reverse side if necessary and identify by block number)

The explosions that most concern us all have effects known mainly by calculation. Since the calculations' credibility influences the cost and scope of deterrence, reliable numerical prediction of explosion-effects is a long-sought goal. For free fields, flaws in stress-strain relations limit the accuracy of predicitions: such relations are hard to establish for specific geo-materials and admit a very wide range of fields. However, the kinds of deformation occurring in free fields depend more on burst geometry than on

DD FORM 1 JAN 73 1473 EDITION OF 1 NOV 65 IS OBSOLETE

UNCLASSIFIED

SECURITY CLASSIFICATION OF THIS PAGE (When Data Entered)

20. ABSTRACT (Continued)

material properties. In particular, for contained, nearly spherical bursts - the basic events in nuclear monitoring - the paths traced in strain space by deforming material elements ("strain paths") have shapes and orientations ("patterns") that vary little with medium. Also, a) the patterns form a simple set, b) at a given strain amplitude they are not diverse, and c) hardware is at hand for stress measurement along them in the laboratory and (probably) in situ. Hence, it now appears feasible to obtain by measurement the stress-strain curves needed for reliable prediction of seismic sources.

A subset of the same curves also prevails on a sizable, downgoing part of the field produced by a surface burst. Further, while paths are more complex and variable near the surface, they may still form a set small enough for stress-strain measurement - though that will not be so if full control over plane strain, including axis-rotation, is needed. Moreover, in surface-burst fields, paths of spherical type give way to plane-strain paths on a transition region for which measurement of stress-strain curves looks impractical. Thus, for surface bursts, mechanistic models must be asked to extrapolate from measured curves - but to a far smaller extent than at present.

Extrapolation with mechanistic models is to be avoided because i) their record of ground-motion prediction is poor, and ii) the predicted effects of their mechanisms on the stress-strain curves traced in explosions have yet to be confirmed. Also, despite its glitter, postdiction is almost useless for model-validation, because infinitely many models will reproduce any given field of motion. However, free-field prediction can be made more reliable - now - by means of strain-path models, in which mechanistic models are used freely for interpolation among measured stress-strain curves. The same curves are needed to validate mechanistic models, whose development (the ultimate goal) is therefore aided by strain-path methods - all the while minimizing unvalidated use of the models for extrapolation.

PREFACE

The work summarized herein was performed over the past decade for the Air Force Systems Command (Norton AFB), the Defense Nuclear Agency, the Defense Advanced Research Projects Agency, and the Air Force Weapons Laboratory. Among the many government personnel whose support, advice and encouragement have been vital to its performance, thanks are due especially to Maj. John Kaiser, Dr. George Ullrich, Col. Donald Gage, Col. George Bulin and Dr. Carl Romney. It is a pleasure as well to acknowledge the assistance of Dr. James Workman, whose comments and draftsmanship were essential in preparing the manuscript, and who has contributed notably to the work itself almost since it began. Also in order are sincere thanks to Mr. Neil Perl for innumerable bits of help along the way, and to Mrs. Barbara Glaser who manages to convert my microscrawl to print.

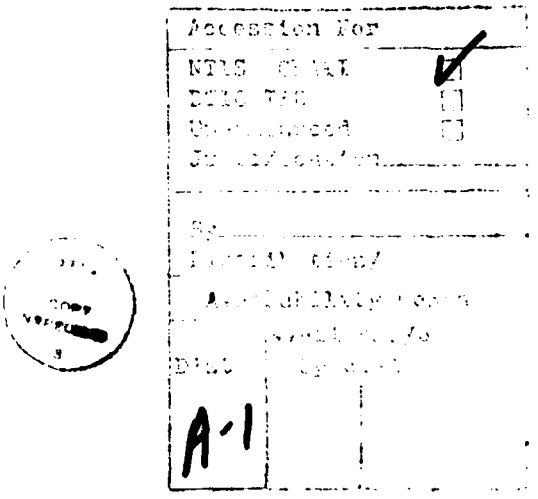

Conversion factors for U.S. customary to metric (SI) units of measurement

To Convert From	To	Multiply By
angstrom	meters (m)	1.000 000 X E -10
atmosphere (normal)	kilo pascal (kPa)	1.013 25 X E +2
bar	kilo pascal (kPa)	1.000 000 X E +2
barn	meter^2 (m^2)	1.000 000 X E -28
British thermal unit (thermochemical)	joule (J)	1.054 350 X E +3
calorie (thermochemical)	joule (J)	4.184 000
cal (thermochemical)/cm^2	mega joule/m^2 (MJ/m^2)	4.184 000 X E -2
curie	*giga becquerel (GBq)	3.700 000 X E +1
degree (angle)	radian (rad)	1.745 329 X E -2
degree Fahrenheit	degree kelvin (K)	$t_K = (t°f + 459.67)/1.8$
electron volt	joule (J)	1.602 19 X E -19
erg	joule (J)	1.000 000 X E -7
erg/second	watt (W)	1.000 000 X E -7
foot	meter (m)	3.048 000 X E -1
foot-pound-force	joule (J)	1.355 818
gallon (U.S. liquid)	meter^3 (m^3)	3.785 412 X E -3
inch	meter (m)	2.540 000 X E -2
jerk	joule (J)	1.000 000 X E +9
joule/kilogram (J/kg) (radiation dose absorbed)	Gray (Gy)	1.000 000
kilotons	terajoules	4.183
kip (1000 lbf)	newton (N)	4.448 222 X E +3
kip/inch^2 (ksi)	kilo pascal (kPa)	6 894 757 X E +3
ktap	newton-second/m^2 ($N-s/m^2$)	1.000 000 X E +2
micron	meter (m)	1 000 000 X E -6
mil	meter (m)	2.540 000 X E -5
mile (international)	meter (m)	1.609 344 X E +3
ounce	kilogram (kg)	2.834 952 X E -2
pound-force (lbs avoirdupois)	newton (N)	4.448 222
pound-force inch	newton-meter (N-m)	1 129 848 X E -1
pound-force/inch	newton/meter (N/m)	1 751 269 X E +2
pound-force/foot^2	kilo pascal (kPa)	4 788 026 X E -2
pound-force/inch^2 (psi)	kilo pascal (kPa)	6 894 757
pound-mass (lbm avoirdupois)	kilogram (kg)	4.535 924 X E -1
pound-mass-foot^2 (moment of inertia)	kilogram-meter^2 ($kg-m^2$)	4.214 011 X E -2
pound-mass/foot^3	kilogram/meter^3 (kg/m^3)	1.601 846 X E +1
rad (radiation dose absorbed)	**Gray (Gy)	1.000 000 X E -2
roentgen	coulomb/kilogram (C/kg)	2.579 760 X E -4
shake	second (s)	1.000 000 X E -8
slug	kilogram (kg)	1.459 390 X E +1
torr (mm Hg, 0° C)	kilo pascal (kPa)	1.333 22 X E -1

*The becquerel (Bq) is the SI unit of radioactivity; 1 Bq = 1 event/s.
**The Gray (Gy) is the SI unit of absorbed radiation.

TABLE OF CONTENTS

LIST OF ILLUSTRATIONS

1. Background and Summary: Overview

To compute the response of the earth to explosions below or near its surface, discrete analogs are written of equations that govern continuum motion. Among them are analogs of constitutive relations that define the mechanical behavior of geologic solids. From the time computers became powerful enough to make such geo-modeling practical (~1955-1960), it has differed in one major respect from other parts of numerical continuum mechanics: The accuracy of model-predictions is limited mainly by defects in constitutive relations. At a time (for example) when computed fields of viscous compressible fluid motion were approaching wind-tunnel accuracy (Kitchens, 1972), critical ad hoc assumptions had to be made about material behavior to account for far simpler motion observed during bursts in material as ideal as dome-salt (Trulio et al, 1975). They still do.

Typically, differences between computed and observed motions have been explained as due to physical processes not included in a given model; typically also, experiments have not been performed to verify such explanations independently of the observations that evoked them (they remain ad hoc). There has thus

accumulated a set of at least ten major model-elements (e.g., non-linear elasticity; the Appendix), each offering modelers wide latitude in matching known motions ("postdiction"); at the outset, there were perhaps four. The many postdictions made to date have, by and large, succeeded - but the reverse is true of pre-shot predictions for the handful of explosive events in which they have been tested against measured motions.

The course being taken to model explosive events is evidently open to criticism, and some of that appears below. However, the aim of this paper is not to carp, but to map a more promising course - one that, in a few years, can either yield reliable predictions of explosively-driven motion or tell us that, in all likelihood, no such predictions can be made.

By way of explanation, suppose that in each prediction-test conducted to date, a given model had proven accurate - correct, say, to within 10-20% in both peak velocity and displacement throughout the regions instrumented. Even then, the model's reliability would be in doubt for a burst differing in gross ways from the test-events (e.g., in burial depth, charge distribution and/or yield); after all, extrapolations commonly disclose the limits of validity of theories (and nature's surprises). However, doubt would largely vanish if the stress-strain curves traced by material in the new (computed) field closely matched those of the previous test-events. Again, if stress-strain curves unlike those seen earlier occurred widely in the new field, they still might prove to be followed closely in the laboratory or - better - in situ; confidence in the predicted field would then approach certainty. On the other hand, the measured curves could differ greatly from those calculated. The causes of the differences would then have to be found by testing one or more of the model's elements under conditions set by the wayward curves - and, after

similar tests of their validity, equations might have to be added to the model to account for physical processes previously ignored.

As matters stand, model-predictions rarely approach the accuracy just presumed. Also, i) the standard data-base for prediction comes from a few laboratory tests in which the stress-strain curves traced run far from those of the fields predicted, and ii) infinitely many stress fields (and hence models) permit exact postdiction of a given field of motion. Hence, standard practice has taken us but a small step toward model validation of the kind just described. Yet, such validation (or equivalent) is vital if conventional methods are to yield models that can be counted upon for accurate prediction of explosively driven ground motion. For, of necessity, the aim of those methods is not simply to make correct predictions, but also to identify each important physical process triggered by explosions, write equations that correctly describe it, and combine the resulting equation-sets in a theoretically sound way (e.g., in accord with the entropy principle). In short, if the predictions of models like those used now are to be trusted, they must be right for the right mechanistic reasons.

Ultimately, correct mechanistic models are the objects sought. How long it will take to find them can only be guessed, but it must be admitted that validating all important model-elements for geo-materials is a major enterprise (the Appendix). Yet, reliable predictions are needed now. To get them, another approach can be taken to modeling which, due to its very empiricism, may also speed the process of mechanism-validation. In particular, study of the stress-strain curves on which attention must center in certifying mechanistic models, has shown that the kinds of deformation material undergoes are a) determined more by burst geometry

than constitutive properties, and b) dominated by a few fairly simple kinds of strain. To be sure, there are limits to the truth of a) and b); however, for deep, nearly spherical bursts those limits are more conjectural than real - and even for surface bursts they lie well beyond the range of validity of present computational models.

Findings a) and b) form the basis of strain-path modeling, whose hallmarks are these: Most of the stress-strain curves needed for accurate prediction of motion at a given site are obtained by measuring stress along the kinds of strain paths already known to dominate explosively driven fields. Mechanistic models are then required to reproduce the measured curves, if they can. If they cannot, then the stress-strain data needed for accurate prediction (having been measured) are forced into them in openly ad-hoc ways. At the same time, their authors are presented, in stress-strain form, with specific conflicts between actual data and their constitutive equations. Any improved understanding that results translates at once into better models for predicting ground motion due to explosive loading - a result that plainly benefits organizations whose missions call for such predictions. Another similar benefit arises in dealing with differences between material in the laboratory and in situ, which pose a basic problem for all modeling: For most strain-paths of the dominant set, stress gauges may finally be at hand with which to quantify those differences, so that sample-and-lab-test procedures can be revised accordingly.

A designer of footings (for example) may see little hope for help in such a program, but it could also be held that better knowledge of the mechanisms of soil response will have across-the-board benefits. Indeed, developing valid special-purpose models of geo-materials could prove an efficient way to arrive at all-purpose models, and strain-path methods may find fruitful application in other branches of materials science.

However that goes, the fact is that even well-tested mechanistic models can fail if used for long extrapolation. Hence, when the jump is made to predicting the effects of a nuclear explosion at a given site, it must also be verified experimentally that the stress-strain curves traced by material in the calculated field really do apply to the material at that site. Fortunately, the job may not have to be done for more than a few sites; the evidence is already strong that strain-path shapes are not greatly altered by a change in source-type from chemical to nuclear (burst geometry outweighs that change). The economic stakes alone easily suffice to justify the cost of such verification.

2. Prediction and Postdiction

On occasion, calculated free-field motion is made available for a given event before it occurs. In that case - if the event does not merely copy an earlier one - a model's predictive power can be tested. A prediction of that sort for the Hudson Moon HE Experiment (Bjork, 1972), proved as accurate as any yet made. The calculated field was spherical, and for practical purposes the actual field probably was also. Predicted and actual pulses from the event are shown in Fig. 1 for the smallest and largest radii of measurement (1.05 m and 3.82 m), and an intermediate one. The outermost gauge may well have been placed at a smaller radius than intended (Bjork, 1972, p.23), but even then calculated pulse-peaks drift below those measured, as radius increases. Indeed, though uncommonly accurate, the calculated pulses as a whole tend to decay faster with range than those measured, from mid-range or less (~1.68 m) outward.

Harder to assess is the decision of the shot's designers to measure radial stress, σ_r; that task, whose subtlety was not

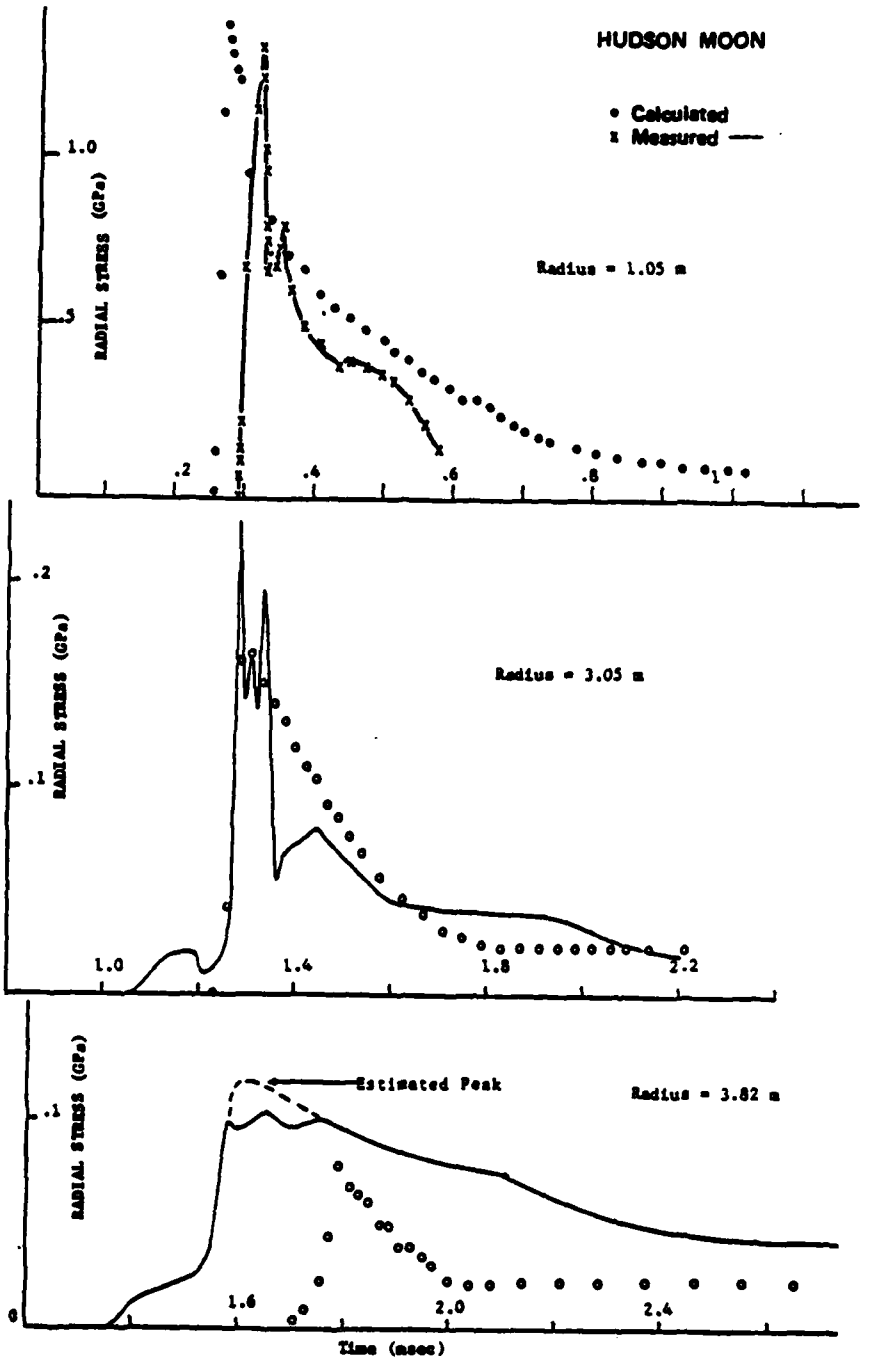

Figure 1. Hudson Moon H.E. Experiment: Spherical Radial Stress vs. Time, Measured and Predicted at Three Distances from the Burst Point.

well understood in 1971, is only now becoming feasible for spherical fields in geo-solids. Nevertheless, these measured stresses could be substantially correct, especially at the smaller gauge-ranges, because they generally exceed by far the material's failure limit, Y_o: $|\sigma_r - \sigma_\theta| \leq Y_o \approx 35$ MPa, in the laboratory [$\sigma_\theta \equiv$ hoop stress]. Thus, over most of the space-time domain of measurement, the medium was more a fluid than a solid. Principal stresses were of course measurable in fluids before 1971, and calculations of fluid motion were quite reliable by then; as already noted, mazy fluid motions have long been predictable using computational models like the ones applied to ground motion problems. Further, while radial stresses at the two greatest gauge ranges were only about as large as Y_o much of the time, motion there was driven by the predictable quasi-fluid field found at somewhat smaller ranges.

The main goal (and problem) in modeling geo-materials is to describe the effects of shear accurately when stress gradients have strong deviatoric components. The match between predicted and measured pulses in the field of Fig. 1, which is especially close at the smaller gauge-ranges, would be clear evidence of such power if octahedral shear stresses at gauge-ranges were about as large as mean stresses. Actually, for the most part, they were much smaller (though a little shear was astutely observed to have sizable effect on mean stress (Bjork, 1972, p.5)). On the other hand, for the Diamond Dust event (also in tuff; Sauer and Kochly, 1971), the maximum possible shear stress, $\frac{1}{2}Y_o$, was greater than a third of the mean stress at even the smallest gauge-range. Also, pulse-amplitudes varied by almost twice the factor seen in Fig. 1 (radial velocity was measured, as usual, rather than stress). Moreover, in the model used to predict Diamond Dust motion, the dependence of mean stress on compression was found from hydrostatic tests alone - whereas a major result of the later Hudson Moon HE

Experiment was that uniaxial strain data are more germane to nearly spherical bursts. Despite these drawbacks, the pulses predicted for Diamond Dust were about as accurate as those of Fig. 1 (Trulio and Perl, 1974, p.48-53). Computed peak velocities did depart from the observed power-law decrease with range, and, at the farther ranges, predicted pulses decayed more slowly than those measured - but the errors were not larger than in Fig. 1. Still, when all the experimental and modeling procedures followed for Diamond Dust were used again for the Diamond Mine event (Sauer and Kochly, 1972), the predicted Diamond Mine pulses were much less accurate than for Diamond Dust (Trulio and Perl, 1974, p.96-107) - although the two bursts took place only 190 m, and 7 weeks, apart. Indeed, even the grout columns that housed the gauges again ran radially outward from shotpoint.

The Piledriver event in Climax granite (1964) came too early in the models' development to make their predictions (if any) informative. Yet, with regard to Piledriver motion (Hoffman and Sauer, 1969), one truly noteworthy point has emerged: To this day, no models can account for it without critical ad hoc assumptions. The Cowboy shots in dome-salt (Murphey, 1960) present an even more striking case in which postdiction is not supported by independent measurements of the host medium's properties. Specifically, before 1975, the models' verdict was that dome salt would behave elastically once it stopped failing in shear. Also, according to all laboratory (Heard et al, 1975) and field (Terhune and Glenn, 1977; Perret 1967) measures of the strength of salt (then and now), no shear failure occurred in the roughly spherical Cowboy fields at radial stresses below 35 MPa. Yet the measured radial-velocity pulses made it clear that deformation was far from elastic at 1% of that radial-stress level. [Note: Early work on the salt problem showed that pore collapse can give rise to highly inelastic decay

of pulses of any amplitude, even for porosities as low as dome-salt's (~1%)(Trulio et al, 1975, p.41-68; since confirmed by others). While no pertinent measurements have been made, that mechanism is not a likely cause of the inelastic behavior seen at low stresses in Cowboy salt, and in almost every geo-material observed at similar stresses during explosions.] Later, the large effects of inelastic decay were starkly displayed for radial stresses >.05 MPa (the lowest Cowboy level)(Trulio, 1978). However, for those studies, the key issue was linearity rather than elasticity (Trulio, 1981a), and laboratory and in situ testing was initiated in 1981 to resolve it. Analysis of the resulting in-situ data has barely begun, but the laboratory answer is this: Deformation is strongly nonlinear in dome salt down to .1 MPa of live stress, and weakly nonlinear (slowly tending toward elastic behavior) as far below that as the data reach (~.001 MPa)(Tittmann, 1983).

Given the fact of inelasticity at low stress, models were adjusted: To better match measured Cowboy motions, Y_o was cut 17-fold to 40 bars (Rimer and Cherry, 1982; the resultant break to linear elastic decay at $\sigma_r \approx 4.5$ MPa remains at odds with both Cowboy motion and the laboratory results above). The rationale for the cut was that dome-salt is water-saturated, and hence has no frictional strength, in accord with effective-stress theory. However, all analyses of Cowboy salt showed that it was very dry; also, many competent persons familiar with the Cowboy medium were consulted and all of them rejected the idea that it was saturated, or even wet (ATI file, 1980). By contrast, saturations well above 90% are needed experimentally to eliminate frictional strength in soils and rocks. Moreover, while effective-stress theory predicts such a loss of strength in materials whose solid skeletons are softer than water, the same loss would conflict with effective-stress theory for rocks of low porosity ($\lesssim$ 1%) - even if 100% saturated - because their skeletons

have always proven much stiffer than water. The same procedure has nonetheless been used to better match Piledriver motion (Cherry and Rimer, 1982).

For surface bursts, prediction began very poorly with events Middle Gust (Wright, Sandler and Baron, 1973) and Mixed Company (Ialongo, 1973), on clay/shale and siltstone/sandstone media, respectively. However, in perhaps the only other documented surface-burst prediction, accuracy approached that of Fig. 1 for the few near-surface pulses computed and reported (Misers Bluff Event II-1; Thomas, 1979). Yet, two caveats are in order, besides the dearth of comparisons between predicted and measured pulses: In the first place, prediction accuracy fell with distance from ground zero, and the extent to which fluid motion was observed out to the two stations of high accuracy is an open question. Secondly, motions were known beforehand for many relevant shots fired earlier on desert soils (five at the Misers Bluff site); what can be left to predict after several similar fields have been measured, is a sticky question that keeps growing in importance (it might best be answered by basing a purely empirical prediction on those fields). Nevertheless, the field predicted for Misers Bluff Event II-1 was much more accurate than those for Middle Gust and Mixed Company. In addition, motion is said to have been forecast well at the edge of the crater dug by a burst on desert alluvium (Mill Race; 1981), and on a grout/wet tuff medium (Mini Jade; 1983); as yet, results are not available in print for either field, but the medium in each was quite likely quasi-fluid from ground zero to almost all gauge stations.

As for postdiction, modelers may have produced an accurate account of motion for Middle Gust Event 3 a few years ago, after i) minor model-adjustments, and ii) sample-and-lab-test procedures were modified, giving rise to major changes in the material properties data-base (the new model and postdiction are

not yet published). However, while defects of a model are disclosed by its postdiction errors, accurate postdiction is all but useless as a measure of its correctness. To see why, let $\sigma_{ij}(\underline{x},t)$ denote stress in a given field at position $\underline{x}$ and time t, where $\underline{x}$ lies on a region enclosed by some surface S; also, let $\sigma^e_{ij}(\underline{x};t)$ be any time-ordered sequence of stress fields i) that satisfy the equation of static stress equilibrium [$\sigma^e_{ij,j}=0$], and ii) whose tractions vanish all over S. It then follows from the equations of continuum motion that the sum of the two stress fields [$\sigma_{ij}(\underline{x},t) + \sigma^e_{ij}(\underline{x};t)$] will produce exactly the same motion as $\sigma_{ij}(\underline{x},t)$; neither the momentum nor density of any material element is affected by the addition of $\sigma^e_{ij}(\underline{x};t)$ to the stress field. [Note: Temperature is affected, but has not been measured; while internal energy and motion do not generally suffice to determine stress, they might in spherical fields.]

For example, exactly the same spherical motion is produced by two stress fields (σ_r,σ_θ) and $(\hat{\sigma}_r,\hat{\sigma}_\theta)$ that differ as follows on the interval $r_1 \leq r \leq r_2$:

$$\hat{\sigma}_\theta = \sigma_\theta + f(r;t) \tag{1}$$

$$\hat{\sigma}_r = \sigma_r + (2/r^2)\int_{r_1}^{r} x\, f(x;t)dx \tag{2}$$

where f(r;t) is any function such that

$$f(r;0) = 0 \quad \text{and} \quad \int_{r_1}^{r_2} x\, f(x;t)\, dx = 0 \tag{3}$$

The first of Eqs. (3) insures that the two fields evolve from the same initial (t=0) conditions; the second dictates that $\hat{\sigma}_r=\sigma_r$ at $r=r_2$ [as at $r=r_1$; Eq. (2)]. The number of functions f(r;t) satisfying Eqs. (3) is strongly infinite, and remains so even if we require i) f(r;t) to be continuous in r,t, and ii) $\hat{\sigma}_\theta$ to equal σ_θ at r_1 and r_2 [$f(r_1;t)=0=f(r_2;t)$].

For general fields, components of σ^e_{ij} are readily found as products of functions of the single Cartesian variables x,y and z:

$$\sigma^e_{11} = A_{11} fg''h'' \quad , \quad \sigma^e_{22} = A_{22} f''gh'' \quad , \quad \sigma^e_{33} = A_{33} f''g''h$$
$$\sigma^e_{12} = A_{12} f'g'h'' \quad , \quad \sigma^e_{23} = A_{23} f''g'h' \quad , \quad \sigma^e_{31} = A_{31} f'g''h' \tag{4}$$

where f(x;t), g(y;t), h(z;t) are any functions twice-differentiable with respect to x,y and z, respectively, and primes (') denote their spatial differentiation; also

$$\sigma^e_{ji} = \sigma^e_{ij} \; ; \quad A_{ji} \equiv A_{ij} \; ; \quad A_{i1} + A_{i2} + A_{i3} = 0 \tag{5}$$

Initial conditions will be unaffected by σ^e_{ij}, and its tractions will vanish over the faces of a rectangular parallelepiped RP at $x=\pm a$, $y=\pm b$, $z=\pm c$, if we require that

$$0 = f(x;0) = g(y;0) = h(z;0) \tag{6}$$

$$f = 0 = f' \text{ at } x=\pm a \; ; \; g = 0 = g' \text{ at } y=\pm b \; ; \; h = 0 = h' \text{ at } z=\pm c \tag{7}$$

If, in addition, $f''=0$ at $x=\pm a$, $g''=0$ at $y=\pm b$ and $h''=0$ at $z=\pm c$, then stress (not just traction) will be continuous at the surface of RP. Thus, for any spatial region in which RP can be embedded (and hence all regions of practical concern), the number of stress fields that will produce identical motions under the same initial and boundary conditions is again strongly infinite.

More general static equilibrium fields are obtained if the arbitrary space-time function $W(\underline{x};t)$ replaces fgh in Eqs. (4); components of σ^e_{ij} then become weighted partial derivatives of W ($\sigma^e_{11} = A_{11} W_{yyzz}$, $\sigma^e_{12} = A_{12} W_{xyzz}$, etc., where subscripts denote

partial differentiation). However, only causal stress-strain relations are strictly admissible, and any stress field consistent with a given field of motion must be tied to the strain field implied by that motion. The added constraint of causality is too broad to discuss here, but enough progress has been made with it to show that there is no limit to the number of causal stress-strain fields consistent with a motion-field.

There are at least two special motions (uniaxial and non-radial-cylindrical) that uniquely determine a single stress component. Otherwise, by forcing a constitutive model to reproduce a given field of motion, we get just one of an infinite set of models that reproduce it. Within said set, departures from the stress-strain curves actually followed in the field can be small, moderate or large. Hence, a constitutive model that does not reproduce the motion observed will generally be more accurate than many models that do (the accuracy of a constitutive model is set by its stress-strain curves, not by the motions those curves imply). The fact that correct postdiction of a field of motion flows from certain mechanistic assumptions therefore cannot rationally be taken as evidence of their validity; the job of validation is not that easy.

3. Strain Paths in Nearly Spherical Fields

The criteria for model-validation are clear (section 1), but only a detailed account of present models and their growth can show how formidable the task itself has become. As an example, recall that flow rules (just one of the models' major elements) have evolved from Prandtl-Reuss form, to the rule "associated" with yield surfaces (via normality of plastic strain increments), to recent rules that forgo normality - slowly growing complexity whose experimental basis has been very difficult to

establish, even in the laboratory. Thus, three hard facts make it unlikely that mechanistic models will soon yield reliable predictions of motion driven by explosions in geo-solids: i) Their record of prediction is poor. ii) Postdiction is unacceptable as a means of validating them. iii) Validation of model-elements one by one for typical materials is a difficult, long-range task that has hardly begun. The ongoing need for reliable predictions - despite these facts - forced us to ask how one might get them even without improved theoretical bases for models. Accordingly, about ten years ago, we re-examined the role of constitutive models in ground-motion prediction.

In calculations of ground motion, constitutive relations serve simply to supply the stress increments produced in material elements as they deform. To the extent that the resulting stress-strain curves do not come from mechanistic models (i.e., from theory), only experiments can furnish them. Of course, the idea of measuring most of the stress-strain data needed in a computational model for reliable prediction seemed wholly impractical. Yet, explosions clearly subject host media to highly specialized loads, and the resulting stress-strain fields should reflect that limitation; stress states in soil under the corner of a building (say) are not produced by a contained, nearly spherical burst in the same medium. We were thus led to ask just what stress-strain data would suffice for the sole purpose of predicting explosively driven ground motion.

An answer was sought at first in terms of the paths traced by material elements in stress space ("stress paths"), mainly because attention in modeling was then focused on yield surfaces. The spectrum of calculated paths was surveyed in terms of path-shape and orientation, or "pattern", since those properties - and

not amplitude - tell us what kind of loading a path represents [for example, states of stress are hydrostatic not because of their amplitudes, but because all three principal stresses are equal in such states (regardless of amplitude), and henee lie in stress space on a straight line whose direction cosines equal $3^{-\frac{1}{2}}$ along normal-stress axes]. The study was halted, however, when it became evident that strain paths, not stress paths, held the answer sought (Trulio, 1975). Once comprehended, the telltale clue to that finding was the similarity of velocity pulses as functions of range, from one deep burst to another, whether measured or calculated, and regardless of medium. Velocity pulses from the Salmon event (Fig. 2; Perret, 1967) illustrate the slowly changing waveform typical of spherical motion from buried bursts; also shown in Fig. 2 are measured pulses of material velocity for bursts in five different media ranging from hard rock to dry soil.

To account for the similarity of the pulse shapes in Fig. 2, we note first that compact energy sources in roughly homogeneous media create nearly spherical fields in which material is first driven outward from the source. Soon thereafter, strong velocity divergence (implicit in spherical symmetry) gives rise to inward accelerations, but inertia carries each material element beyond its final position before its outward movement is arrested. Then, following some inward motion, spherical convergence leads to outward acceleration, etc. In elastic media, the resulting radial oscillations about final positions are heavily damped by the loss of radiated energy; even stronger damping occurs in the inelastic media nature offers. Thus, radial velocity pulses from deep shots consist of an initial positive lobe (outward motion), a negative lobe of lower amplitude, and not much else.

An increase in negative-lobe size with radius, relative to that of the positive lobe (Fig. 2; Salmon pulses), is also quite

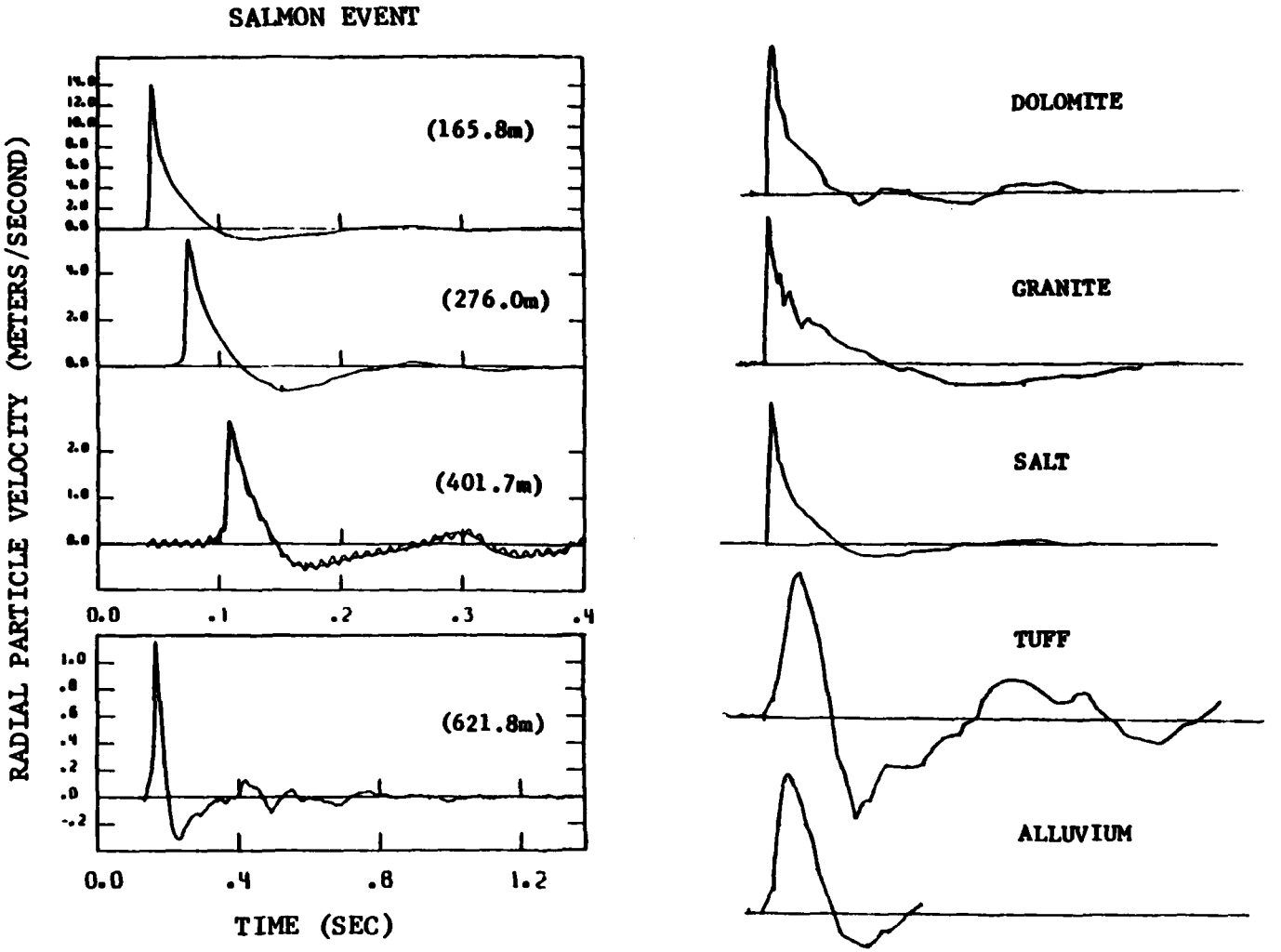

Figure 2. Measured Wholespace Motion: Radial Particle Velocity vs. Time in Fields Thought to be Spherically Symmetric. Left: pulses at various distances from the center of the Salmon burst in dome-salt. Right: one pulse from each of five buried bursts in different media.

general. In elastic media, velocity pulses (being transients) decay in amplitude in proportion to 1/r, while permanent displacements decay as $1/r^2$; the opposed displacements effected by each of the two velocity lobes therefore become more nearly equal in size as range increases. In real geo-materials, outward displacements are largely inelastic where strains are large (small radii), heightening the effect in question - and the tendency of materials to become more nearly elastic with decreasing stress-strain amplitude makes the effect almost universal (despite its multiple mechanistic causes).

For bursts in different media, similar pulses of velocity, U, and hence of displacement, D, powerfully impel strain fields toward similarity (how strongly will soon be seen, but note that hoop strain in a material element is very nearly D/r, while radial strain is roughly equal to U/c; c≡ longitudinal wavespeed (Trulio, 1977; Workman et al, 1981, p.23)). Once that basic point was grasped, emphasis shifted quickly from stress to strain. For, if strain-path patterns are not medium-dependent, then stress-path patterns must be: For example, as long as a radius of observation remains large relative to the length of wavetrain outside that radius (and to displacement), the strain there will be virtually uniaxial. However, stress is then not so constrained or simple. Even during initial shock loading and unloading, stress-path patterns can be quite different for elastic media (say) than for bilinear (hysteretic) ones - and while the former paths (like strain paths) are straight lines, their orientations vary with Poisson's ratio (Trulio, 1981b, p.36-10). Attention also shifted from stress to strain because stress-history is uniquely determined by deformation-history, but not the reverse (non-uniqueness attends yielding); moreover, when different strain paths produce the same stress path in a set of material elements, the properties of those

elements can thereafter differ greatly. In short, specifying stress paths is not adequate to determine the stress-strain curves followed by material in a given field.

Since strain-path patterns do not recur precisely in different media, no strict theorem can underlie the physical plausibility (above) of their near medium-independence. For instance, strain-path fields are exactly known around suddenly-pressurized spherical holes in linear elastic isotropic media, and they vary with medium (loc. cit.). Hence, to quantify the similarity of strain-path fields, the fields themselves had to be examined. In so doing, the shift from stress to strain had critical practical effect: Strain paths in situ can be deduced from measured ground motions, whereas gauges for measuring stress in situ are still under development. In particular, the slow change in waveform with radius seen on the left of Fig. 2, and the smooth (if rapid) fall of amplitude with range, make accurate interpolation possible among pulses differing in radius by a factor of two or more; from discrete pulses, material velocity is thus calculable as a function of range, and with it displacement-, and hence strain-, fields. At least two interpolation procedures are in use (Seaman, 1974; Workman et al, 1981, p.9), but the set of strain paths obtained from gauge output is nonetheless small because not many events have yielded pulses adequate to define their velocity fields. Fig. 3(A) contains paths from those events, which took place in granite, dome-salt, a desert alluvium (Perret et al, 1963), and an ash-flow tuff. Given spherical symmetry, strain paths can be defined in full by plotting hoop strain (ordinate) vs. radial strain (abscissa). However, for the reason cited above, only path patterns (shape and orientation) are so displayed in Fig. 3; in any one plot on its left, strain amplitudes vary as much as a factor of 5 (peak velocities on the right of Fig. 2 span a factor of ~40).

The events contributing to Fig. 3(A) include nuclear and

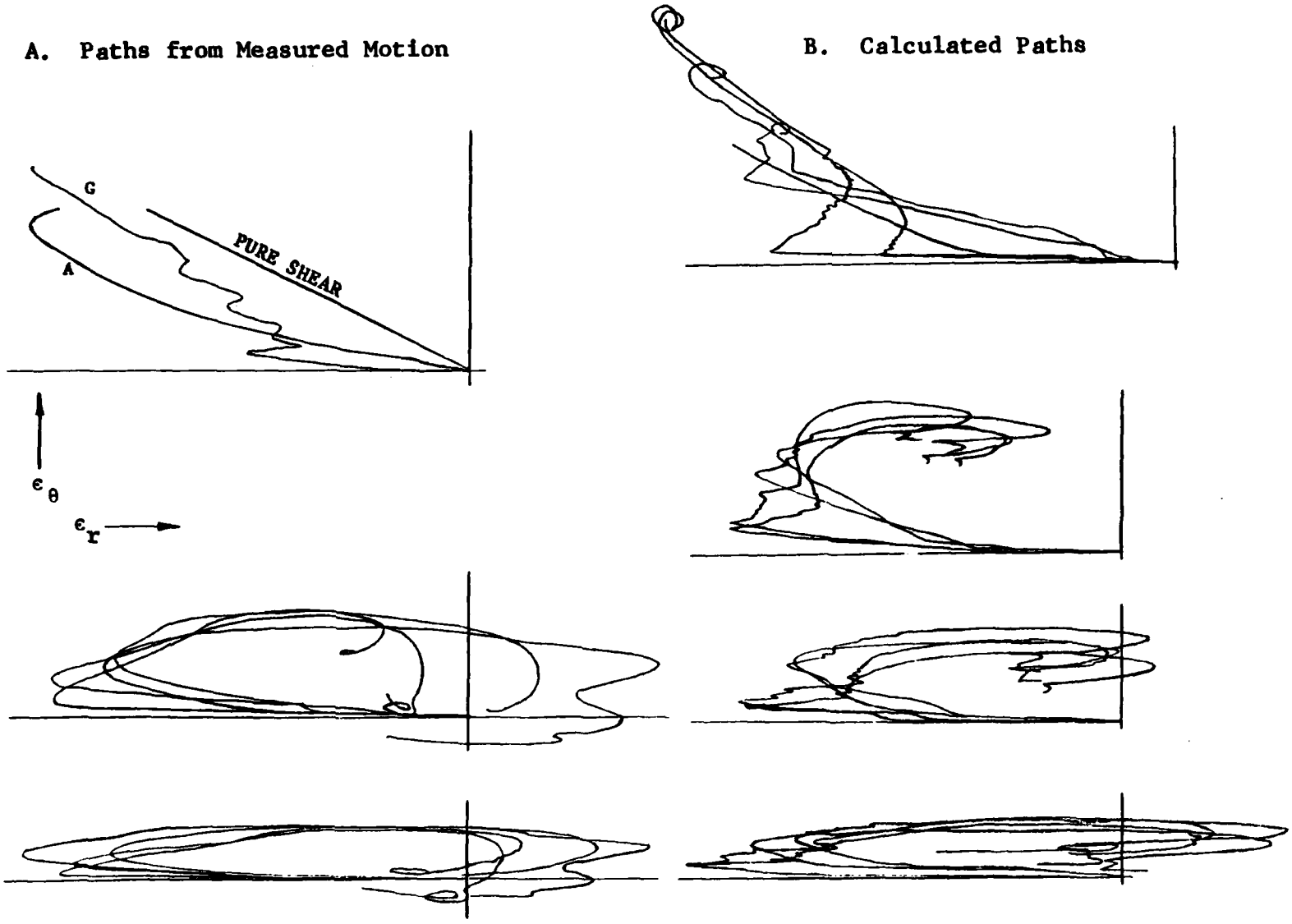

Figure 3. Strain Paths Deduced from Measured Motions in Various Media (left), and Calculated Strain Paths (right), Assuming Spherical Symmetry. Hoop strain, ϵ_h, is plotted vs. radial strain, ϵ_r. On the left, the topmost curves refer to granite (G) and alluvium (A), and the others to tuff and dome-salt.

chemical bursts, each in both tamped and cavity settings. Care was taken to obtain (by eye) matching patterns for the two lower plots, though closer matches are possible. The largest pattern-differences occur toward the ends of paths, but those are the paths' shakiest parts; ground motion gauges are prone to register non-zero final velocities or "baseline shifts", whose correction (as in the pulses of Fig. 2) always entails guesswork. In the upper plot of Fig. 3(A), pattern matching was minimal because granite's velocity field was defined by just the two best-certified wholespace pulses for that medium (Piledriver event); further, the use of those pulses to define spherical motion may be improper, since large nonradial motions were measured for Piledriver (Trulio, 1981b, p.12-12). Calculated spherical fields, of course, have perfect symmetry, and discretization error has negligible effect on strain paths, even at their ends. Also, though unreliable for prediction, constitutive models do describe materials whose behavior tracks that of real ones. Hence, in testing the thesis that strain-path patterns are only weakly medium-dependent, the paths from calculated fields (Fig. 3(B)) are almost as useful as those of Fig. 3(A). The patterns in Fig. 3(B) (none was calculated for granite) scatter more than in Fig. 3(A) because little was done to match paths from different fields; scatter more like that of Fig. 3(A) was seen when, for one of the plots, paths were matched more carefully.

Fig. 3 defines, almost in full, the patterns found in nearly spherical fields driven by single charges. At ranges beyond the greatest in the figures, the already flat paths flatten further, approaching the axis of radial uniaxial strain. Moving inward, hoop-strain-amplitude grows relative to radial-strain-amplitude, and the loops become rounder; they also open steadily, as decreasing fractions of peak outward displacement are recovered (negative lobes of the radial velocity pulses shrink relative to positive ones; above). At smaller radii than in Fig. 3, there

is little further change in path pattern: Large outward displacement of a spherical shell gives it both tensile hoop strain and compressive radial strain that exceed even its initial compressive radial strain (uniaxial) due to shock loading; later, radial and hoop strains dwarf cubical dilatation, whence strain paths become curves of almost pure shear (a straight line of slope $-\frac{1}{2}$ in Fig. 3, if natural strains are plotted).

The empirical evidence that strain-path patterns are similar regardless of medium and source type (Fig. 3) is telling, though not profuse. Beyond that, the case for strain-field similarity has been strengthened greatly by showing that burst geometry underlies it. Summarizing the key points (above): For reasons that are mainly geometric, a) the radius-vector is a strain axis and the other two principal strains are equal, b) point-like sources quickly radiate energy away into a surrounding wholespace, forcing simplicity on velocity waveforms and hence on strain-path patterns, c) only uniaxial strain is seen at large radii, d) at small radii, strain is at first nearly uniaxial and then changes to nearly pure shear, and e) recovery from peak outward displacement becomes more complete with increasing radius, whence (plotting hoop strain vs. radial strain) open paths [d)] gradually become closed flat loops [c)]. Within these constraints, path patterns are most medium-specific during initial straining, and on open paths. For stiffer, more elastic materials, uniaxial radial compression is then partly relieved before geometry forces further radial compression. However, the effect is plain in Fig. 3(B), muted in Fig. 3(A), and hence may demand a degree of elasticity scarce in real geo-materials.

That the paths traced in different bursts and media are similar is a result of signal importance. To the extent that their patterns are the same, the deformations they represent become independent of source and medium. So, therefore, do the kinds of material

properties tests needed to supply stress-strain curves sufficient for reliable prediction. Also, since the path-patterns in those tests form a simple set, interpolation among them may be accurate even if only a few are traversed. True, amplitude can be uncertain by as much as an order of magnitude for a given path-pattern, but mainly because path-shape (like velocity waveform) is insensitive to amplitude: Using peak-strain-ratio (hoop/radial) to measure the shapes of paths with radial-strain recovery of 50% or more (as in all but the top plots of Fig. 3), shape was found to vary by a factor <2 at fixed amplitude (Fig. 4; Workman et al, 1981, p.33); variability of shape for open paths (Fig. 3; top plots), though less well studied, appears no greater than for closed ones. Hence, the present matrix of strain-path tests calls for stress measurement on two or three different paths for each amplitude of a set that covers a range of interest. In practice, the number of tests can probably be cut even now by forming separate test-matrices for soil, soft rock and hard rock. Moreover, while tests have yet to be made over a full matrix, stress has been measured at a few laboratories on typical paths, both open and closed (Ko and Scavuzzo, 1981; Bogart and Schatz, 1982; Akers, 1983; Lade, 1983). Thus, with present hardware and knowledge of strain paths, it now appears feasible to measure all that needs to be known about material properties for accurate prediction (not just postdiction) of spherical motion around buried bursts - if the resulting stress-strain curves apply to geo-materials in situ.

This last issue cannot be decided short of in-situ measurement of stress-strain curves. Strain is accessible in nearly spherical fields (above), but in-situ stress measurement is frustrated by the conflicting requirements that, at gauge faces, both tangential straining of the medium and its shear stress be unaffected by the gauge. After years of development, gauges are now becoming operational that can, in principle, record a principal free-field stress without serious distortion, if the allied stress-axis is fixed and

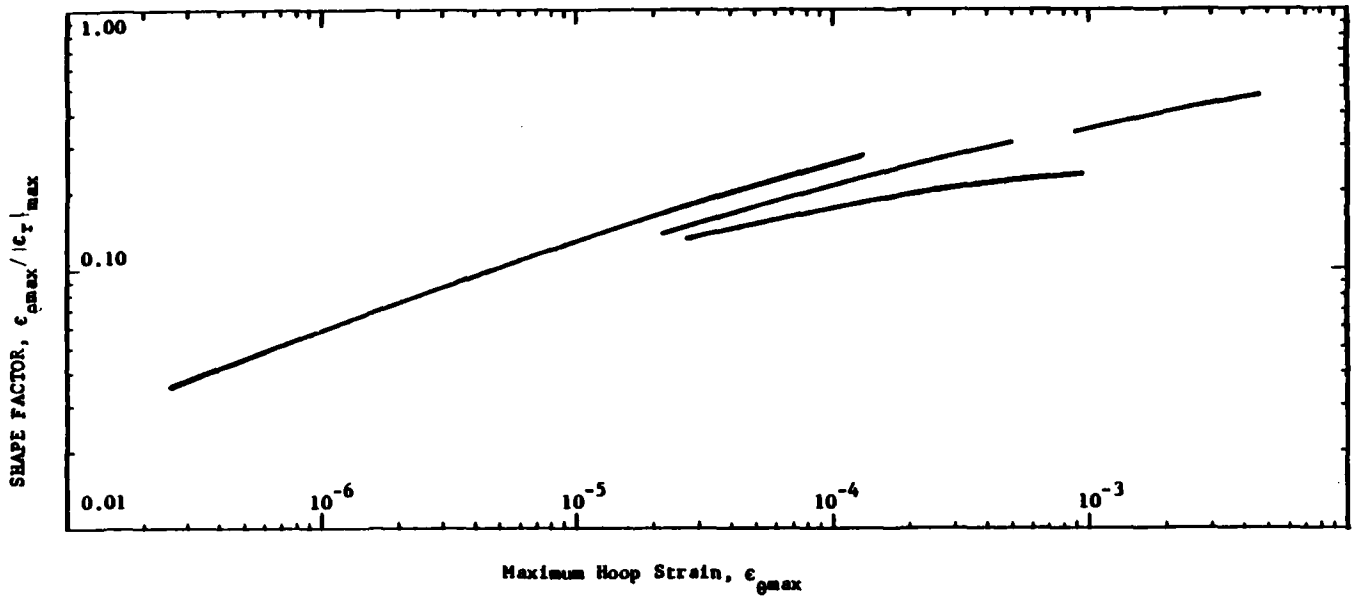

Figure 4. Shapes of Strain Paths as Functions of Maximum Hoop Strain, Deduced from Motion Measured in Fields Considered Spherically Symmetric. Shape is defined as the ratio of maximum tensile hoop strain, $\epsilon_{\theta max}$, to maximum compressive radial strain, ϵ_{rmax}, excluding paths like those in the top row of Fig. 3.

known (Keough, DeCarli and Rosenberg, 1976). Those gauges were exercised very recently, along with ground-motion gauges, in the field of a buried spherical charge. Earlier, using samples of the medium near the charge, stress had been measured in the laboratory along expected strain paths; similar measurements will be made on strain-paths that the ground-motion records imply at stress-gauge locations. The test plan also calls for calculation of the impulse delivered to material elements (using stress-gauge output) and the momenta of those elements (using motion-gauge output); the fractional difference between impulse and momentum can presumably be ascribed to errors in stress-gauge output. To that accuracy, differences between lab and in situ behavior will then be known, and sample-and-lab test procedures can be modified in order to reduce them.

4. Strain Paths in Axisymmetric Fields: Surface Bursts

At the next level of complexity - but a long step up - lay axisymmetric fields calculated for surface bursts on layered and homogeneous media. Yet, study of those fields soon showed (Workman et al, 1978) that they were much simpler, in one respect, than for general torsionless axisymmetric motion (i.e., with no rotation about the symmetry axis): Near the ground surface, at distances $\gtrsim$1.5 crater radii from the burst, hoop strain is the smallest principal strain by a factor almost always >4 and usually >8; for the few pertinent strain paths that have been measured, the factor is larger still. Hence, in the region noted, deformation can be approximated as plane strain (no hoop strain). Strain paths then do not wind and twist through principal-strain space, but occupy just a single plane; for any material element, the hoop-strain axis is normal to that plane, which, in physical space, therefore runs parallel to the plane A that contains both the element and the axis of symmetry. As in

the case of strain paths for deep bursts, this simplification too has geometric roots: When a wavetrain passes through matter, torsionless axisymmetric motion becomes planar as horizontal range becomes large relative to wavetrain-length (and to displacement).

In plane A, the more compressive principal strain and the more tensile are denoted ϵ_- and ϵ_+, respectively; hoop strain $\equiv \epsilon_h$. The upper left-hand plot of Fig. 5 shows, typically, that ϵ_h is small near the surface in calculated fields, relative to ϵ_+ or ϵ_-. However, with ϵ_- as abscissa and ϵ_+ as ordinate, near-surface strain paths present patterns much more diverse than those of deep bursts. The kind of pattern seen most often (over 3/4 of the time) - also represented in Fig. 5 (top, center and right) - starts with compressive, nearly-uniaxial strain (along the ϵ_--axis); then, slight-to-full uniaxial recovery is cut short by a cross between pure shear and uniaxial stretch (along the ϵ_+-axis). Such overall patterns are often the net result of many brief excursions about them, in which discretization error plays no small part. On the few paths measured, uniaxial stretch prevails over pure shear, and there are relatively few jogs about the overall path-direction (Fig. 5, upper right); strain axes rotate through a large angle during the switch to uniaxial stretch (which thus can even amount to a final stage of initial uniaxial strain, though we see no reason to expect paths that simple).

The strain-path qualities noted are expecially in evidence up to the time, t_D, when peak downward vertical displacement occurs. That period has been one of prime concern over free fields. Until time t_D, simple strain paths are found over most of the field and not just on its near-surface region. In particular, let the field

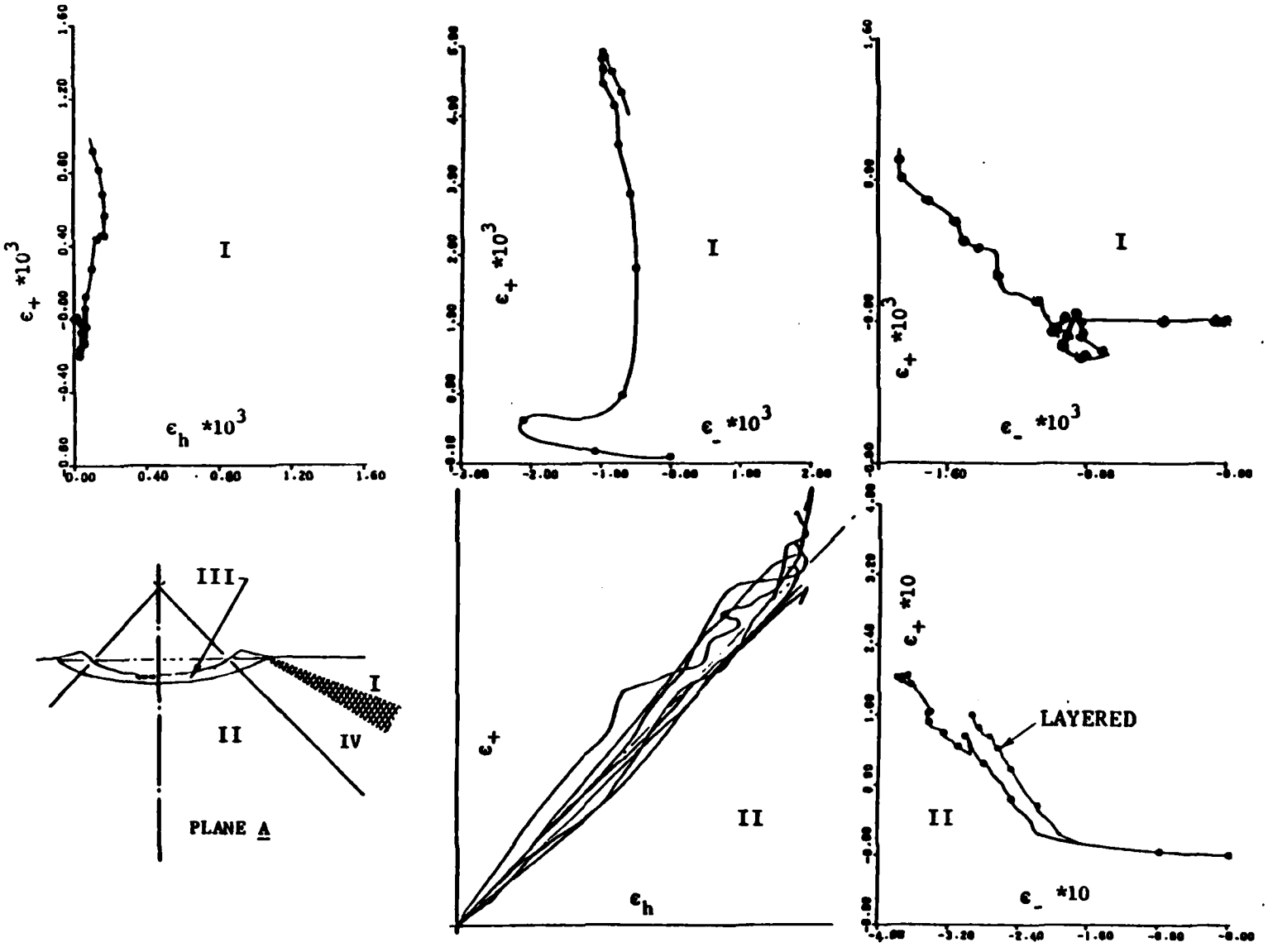

Figure 5. Surface Bursts: Principal Regions of Deformation (lower left) Assuming Axial Symmetry about the Vertical through Ground Zero. Typical paths in principal-strain space are shown for Regions I and II. Hoop strain $\equiv \epsilon_h$, while ϵ_+ is the more tensile of the other two principal strains.

be divided into two parts by a right circular cone, C, that opens downward and has a vertical axis, a half-angle of 45^{o}, and a vertex above the burst point at a height of one crater radius (Fig. 5, lower left; Trulio and Port, 1982). The near-surface region, denoted "I", lies entirely outside C. Inside C and down to about ten crater depths (region II), the paths followed up to time t_D are open ones like those generated by deep bursts (section 3 above) except that compressive uniaxial strain is followed not by pure shear, but by a combination of shear and volume expansion; for both layered and monolithic sites, Fig. 5 shows that, on region II, patterns in the (ϵ_-,ϵ_+)-plane (lower right) do resemble those at the top of Fig. 3, and that $\epsilon_h \approx \epsilon_+$ (bottom, center). We note also that inside C (except for a small region where ejecta form), peak displacement and peak vertical displacement both occur at time t_D. While these results hold for all calculated fields known to us, pertinent measurements on region II are being attempted for the first time in an explosive event, as this is written.

Strain paths are depicted in Fig. 6 over a key part of a field calculated for a chemical burst on monolithic desert "alluvium". Paths like those just deemed typical of region I, and likewise II, are evident in the figure; not shown, but verified, is near-equality of ϵ_h and ϵ_+ for the plots that apply to region II (e.g., one path of Fig. 5 (bottom, center) belongs with those plots). On a given path, "v" marks the point of peak downward vertical displacement due to initial loading and relief; larger downward displacements occur much later in a few cases and point v was not reached in a few others. With rare exceptions motion grows more complex as it unfolds, and discretization error probably accounts more and more for the paths' detailed wriggling. However, it is not known how exact paths for the problem posed differ from these, because a) exact solutions to such axisymmetric problems are lacking and b) time-

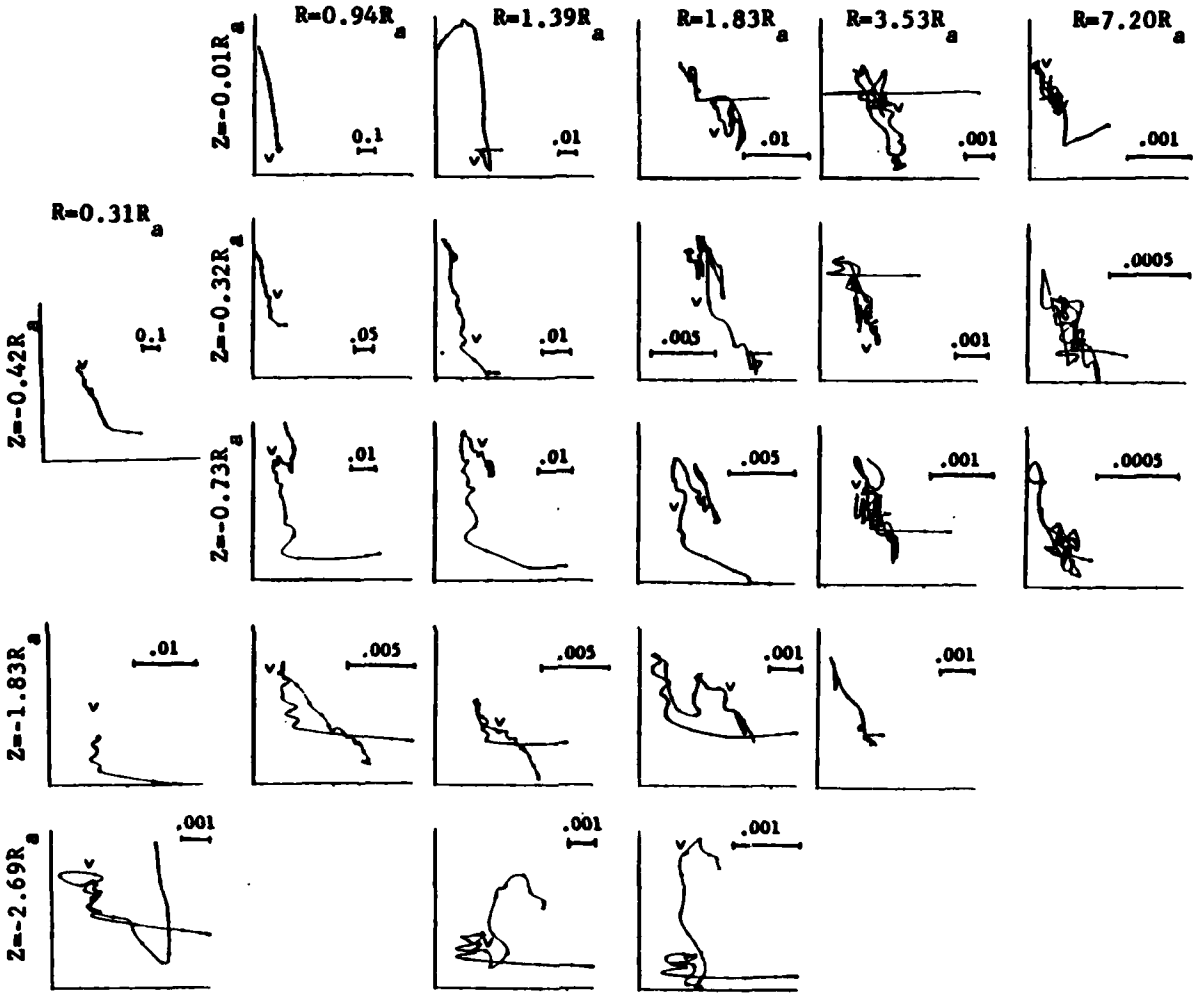

Figure 6. Calculated Principal-Strain Paths for a Chemical Explosion on Monolithic Alluvium. The strain axes lie in Plane A of Fig. 5; ϵ_+ is the more tensile of the two principal strains in that plane. Peak vertical displacement occurs on each path at point "v". Horizontal range, R, and altitude, Z, are given in units of the apparent crater radius, R_a. Strain scales are defined on the horizontal line-segment in each plot (.0x≡x%); dots on any path mark equal time increments.

marching methods give numerical fields whose slow, non-uniform convergence makes it very expensive to put close bounds on their errors by mesh refinement. Larger errors than in Fig. 6 are likely to enter the paths of Fig. 7, which were calculated for a layered alluvial halfspace. While most patterns in Fig. 7 still show typical region-I features beyond time t_D, they tend to be more elaborate than in Fig. 6 even to that time; layering no doubt has such an effect, in which case the effect itself is an added source of numerical error.

Measured motion is also subject to error, and to the further realities of local inhomogeneity and global asymmetry. Still, in the main, we obtained strain paths like those connected above with region I when the first (and only) attempt was made to measure them in situ (Trulio, 1982). For that purpose, a cluster of gauges was deployed around each point M of strain-path measurement: Horizontal and vertical velocities at three points of the plane A (above) define a spatially linear field over the triangle formed by those points - and hence an instantaneous strain rate at M. Since redundancy is needed both as a hedge against gauge failure and for error assessment, each cluster actually contained four gauge-pairs, giving it a maximum output of sixteen ideally redundant paths. Six clusters were emplaced at the same small depth along two horizontal lines, 2½, 3-3/4 and 5 crater radii from the burst. Over the 44 paths actually obtained after gauge attrition, initial uniaxial strain was clearly followed on 20 by uniaxial stretch, on 6 by shear, and on 5 by a mixture of shear and stretch; as many as 13 had unexpected shapes (of those, all but 2 were computed using one suspect gauge-record or more; most of the gauge canisters proved to be incompletely grouted to the medium, but no relation was seen between bonding and gauge-record-quality; also, as measured by one extra gauge in each cluster, hoop motion was not significant).

A sizable and unvarnished sample of the measured paths is

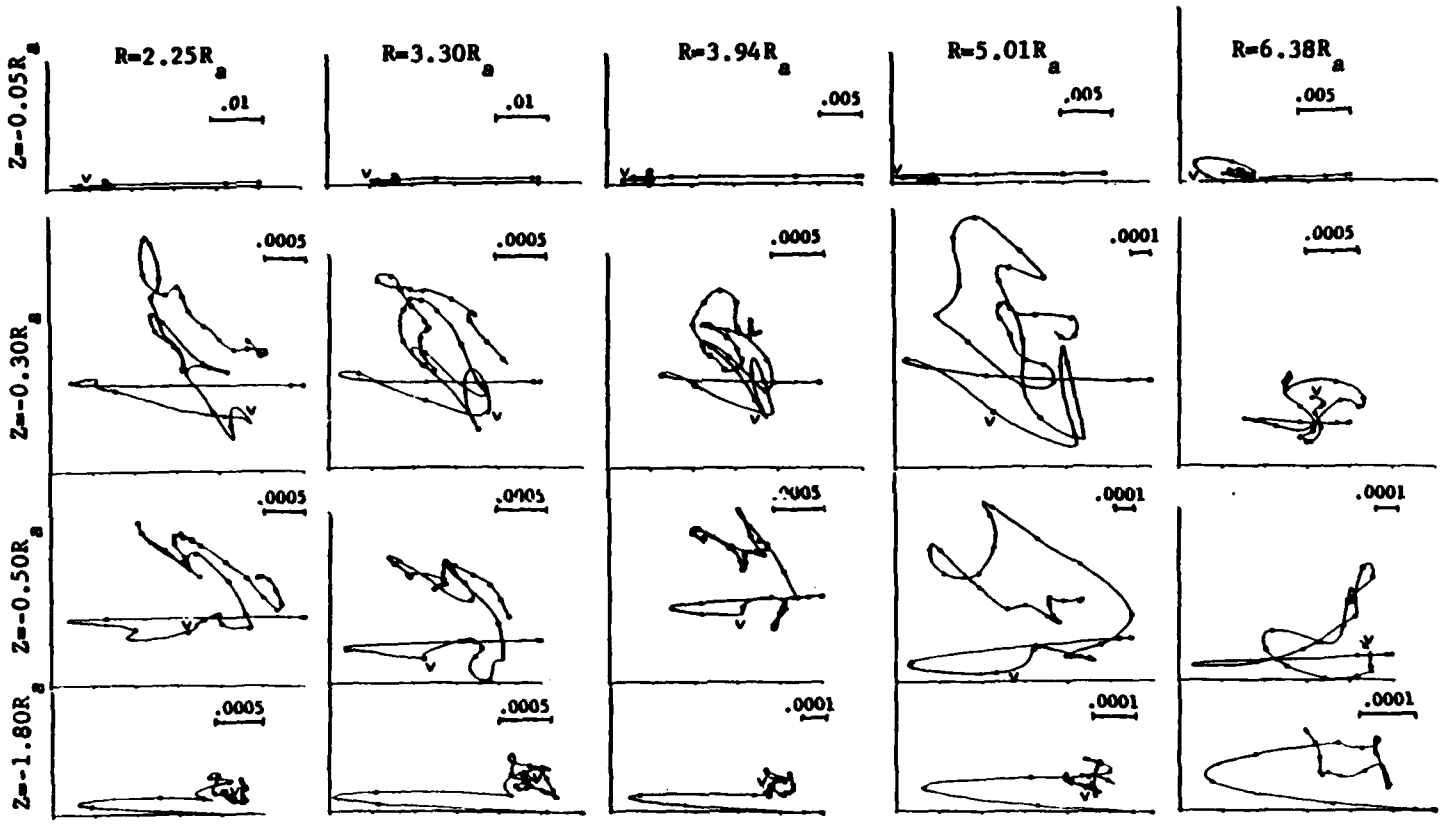

Figure 7. Calculated Principal-Strain Paths in a Layered Halfspace Loaded by Nuclear Airblast. The notation and conventions of Fig. 6 are used here. Layer materials include clay, sand, shale, sandstone and siltstone.

shown in Fig. 8. The top and middle rows of the figure, respectively, contain ideally redundant paths from clusters on the same line, 2½ and 5 radii from the shot; the two leftmost paths on the bottom row came from the central cluster on that line, while the rest are from different clusters on the other line. The one (ϵ_+, ϵ_h)-path shown for each path location of the figure is typical of the clusters in that row (the curve at the bottom right and the one next to it are orthogonal projections of the same path). The similarity between most (ϵ_+, ϵ_-)-paths of this set, and those of Figs. 6 and 7, is plain, and one of their more notable differences is pleasing: the measured paths are less spastic than those calculated.

Ejecta come from the upper reaches of a "crater region", denoted III in Fig. 5, of the same shape as the apparent crater but having 1.5 times its radius and depth. Up to time t_D, region III bears such high overpressures in nuclear bursts that shear stress can probably be ignored there for many media; if so, then plate-slap and hydrostatic experiments in the laboratory can supply the region's essential constitutive properties. Moreover, the methods used to measure stress-strain curves for deep bursts (section 3) should serve equally well in region II. On region I, however, it is much harder to measure strain (as just seen), while laboratory measurement of stress is essential because (like strain) it has fixed, known axes only in the hoop direction, and very close to the symmetry axis.

Observed axis-rotations on region I, which are plotted in Fig. 9 for each (ϵ_-, ϵ_+)-path in the two top rows of Fig. 8, again follow a general pattern. That pattern covers a host of detailed shapes, and is not fit by some rotations, but is nonetheless widespread and distinctive enough to restrict sharply the kinds of stress-strain curves needed for surface-burst prediction. Specifically, the angle θ from the upward vertical in plane A to the ϵ_--axis

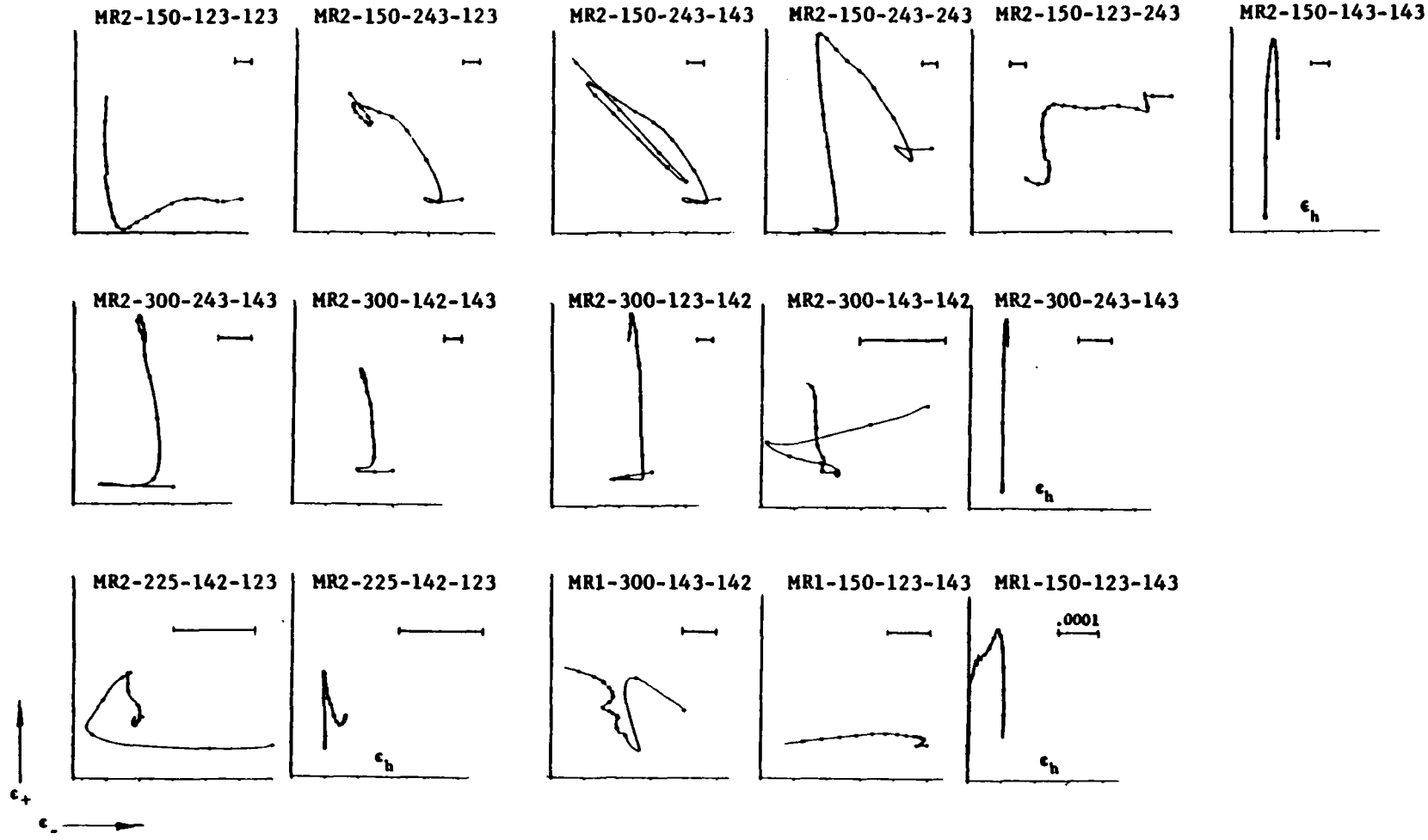

Figure 8. Measured Principal Strain Paths for a Chemical Explosion on Dry Desert Alluvium (Mill Race Event). Hoop strain $\equiv \epsilon_h$; ϵ_+ is the more tensile of the other two principal strains (ϵ_-,ϵ_+). As ordinate, ϵ_+ appears in every plot; plots with ϵ_h as abscissa are so labeled, and the abscissa is ϵ_- in all other cases. Field locations are designated by the first four digits of the path label; e.g., MR2-300-243-143 applies to a point on gauge-line 2, 300 feet (4.8 apparent crater radii) from ground zero. Lines 1 and 2 are 89^o apart and all points of strain-path measurement are 6 meters deep. Except for the lower right-hand plot, the horizontal line-segment in each plot defines a strain of .001 (.1%).

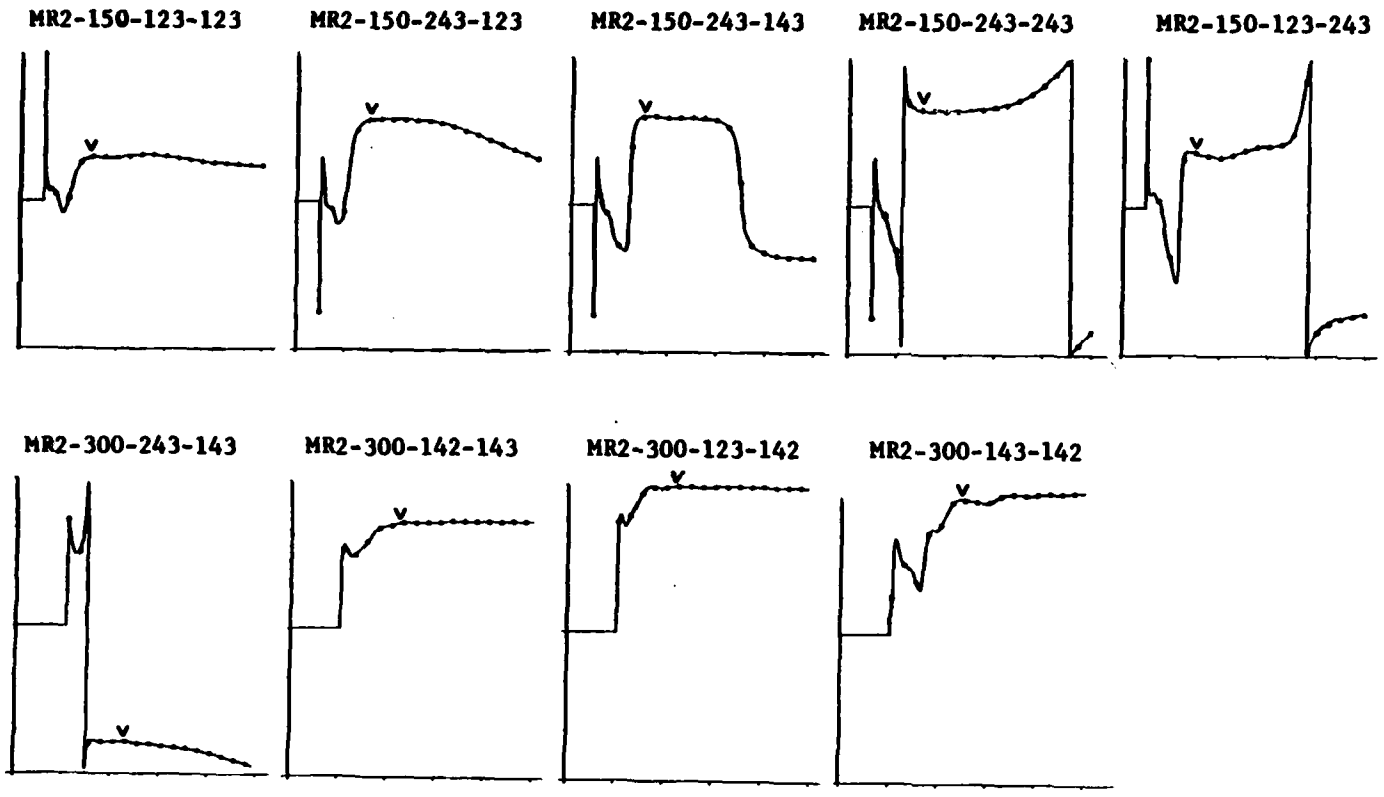

Figure 9. Measured Rotation of Strain Axes in the Vertical Plane through both Ground Zero and any Given Point of Strain Path Measurement (Mill Race Event). Axial symmetry is assumed about the vertical, V, through ground zero. The rotation angle θ is measured from V to the axis of most compressive strain. A plot is shown for each strain path in the top and middle row of Fig. 8, peak vertical displacement occurs at about the point "v".

quickly assumes a value θ_o dictated by the normal direction to the wavefront (only $\theta-\theta_o$ matters; the vertical is an arbitrary reference line). Then θ decreases to a minimum θ_{min}, and increases to a value $\theta_{max}>\theta_o$ that persists until well after time t_D. The angles $\theta_o-\theta_{min}$ and $\theta_{max}-\theta_o$ vary from path to path, as do the (ϵ_-,ϵ_+)-changes subtended by θ_o, θ_{min} and θ_{max}. In fact, the basic pattern in the (ϵ_-,ϵ_+)-plane (Figs. 6-8) itself contains variables - principally amplitude, degree of recovery from initial uniaxial compression, and the proportions of pure shear and uniaxial stretch in subsequent deformation. Thus, on balance, path variations in region I appear too diverse to be covered fully by interpolation among measured stress-strain curves. Moreover, to force material around given plane-strain paths when axes rotate, is beyond the state of the art. Even in the laboratory, stress can be measured only on prescribed principal-strain paths (though of quite general shape). Indeed, up to now, models of geo-materials have all been based on stress-strain tests with fixed stress and/or strain axes; the models' ability to deal with axis-rotation has not yet been put to any direct test - a large gap in model validation.

Even before laboratory equipment is developed to effect prescribed rotations of plane-strain axes, stress can be measured in situ on principal-strain paths like those of Figs. 6-8, and compared to corresponding laboratory data. In particular, Cylindrical In Situ Test (CIST) events generate such paths when they drive cylindrical radial motion. In each of the many CIST events to date, chemical explosive filling a borehole has been detonated all at once (ideally) along its vertical centerline. On any plane bounded by the centerline, a roughly triangular region T is formed by that line and two others, namely, the lines on which a first-arriving wave from the cavity meets first-arriving waves from i) the ground surface, or ii) the bottom of the charge-hole. In a

homogeneous medium of suitable isotropy, radial cylindrical motion lasts at each point of T for a time proportional to the length of explosive. Such motion proceeds in stages much like those outlined above for spherical fields near charges (section 3), but with one basic difference: No two principal strains are equal; instead, one of them (vertical) is zero, and only plane strain occurs. Thus, the initial stage of compressive radial strain (ϵ_-) and possible uniaxial recovery, gives way to hoop stretch (ϵ_+), in qualitative agreement with the typical region-I pattern.

To obtain paths at points of T, we turned to two computed fields (few pulses have been measured on T in CIST events). The two fields differ in the pressures reached by their assumed explosives (noted in Fig. 10). Figs. 8 and 10 make quite plausible the use of CIST events to generate (ϵ_-,ϵ_+)-paths like those of region I; further, since stress axes are fixed and known where such CIST paths occur, stress can be measured there. Hence, while new hardware is needed to deal with strain-axis rotation, only paths on region IV (a zone of transition between spherical and plane strain) appear unsuited to stress-strain measurements.

5. Agenda for Strain-Path Modeling

For surface bursts, the near-term goals of strain-path work are i) to better define the bounds of regions I-III and the paths found on those regions, ii) to pare the set of path-shape parameters that now apply to each region (e.g., by finding relations among them), and iii) to divide geo-materials into classes (e.g., soil, soft rock and hard rock) within which strain paths form relatively simple sets. For these purposes, calculations can be almost as effective as measurements, and offer timely access to fields in highly diverse media. Still, strain paths must also be measured in situ, if only to confirm more fully that burst geometry is the main

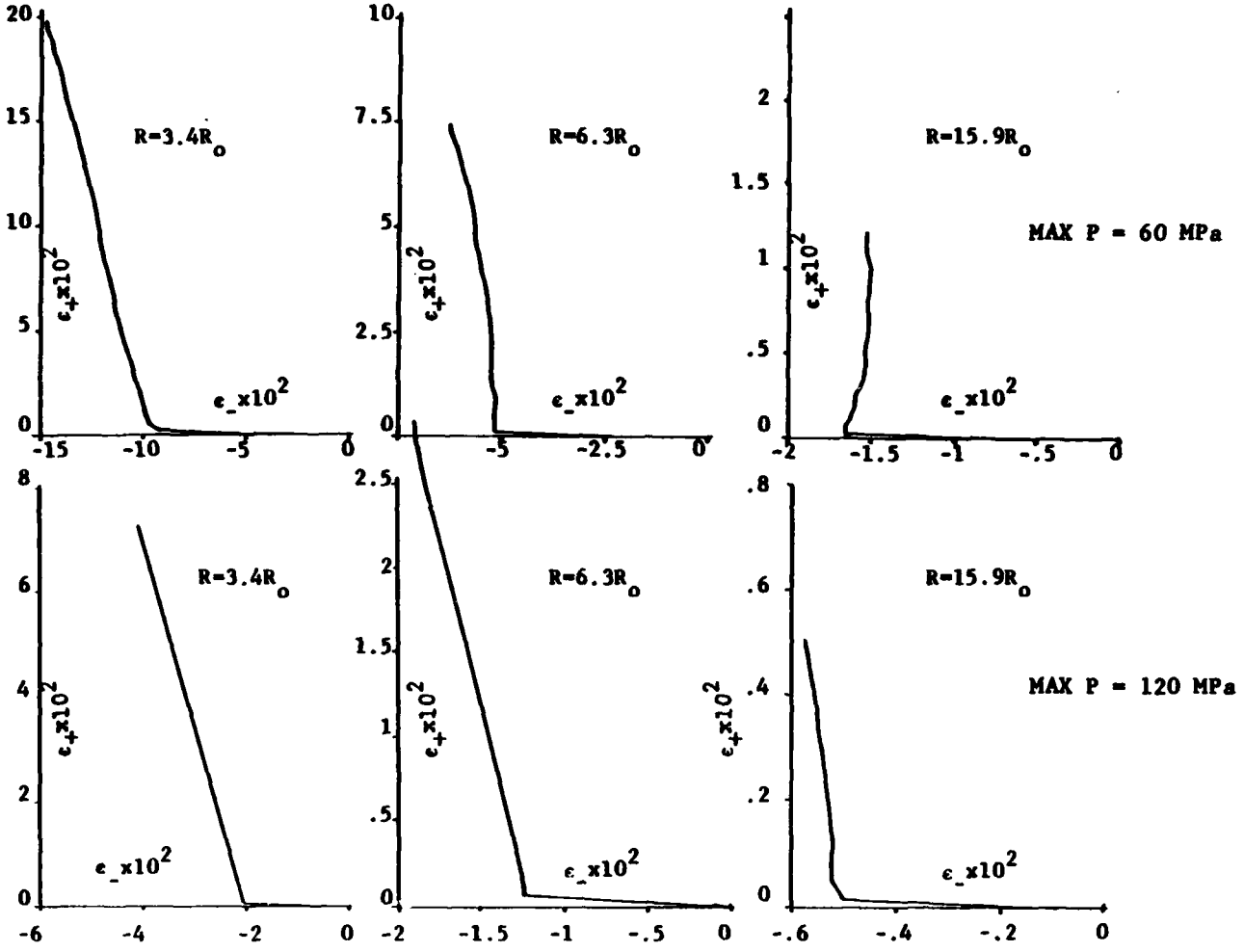

Figure 10. Strain Paths in Cylindrical Radial Fields Driven by Chemical Explosions. Motion is the same in all planes normal to a fixed vertical line, and is radially directed from that line. In any such plane, ϵ_+ and ϵ_- are hoop and radial strains, respectively. The paths on the first and second lines refer to fields driven by explosives with peak pressures of 60 and 120 MPa, respectively.

determinant of their patterns. That task, and also the day of reliable models, would be speeded if strain paths were measured in situ by a simpler, cheaper scheme than the cluster method - but one no less clean in principle.

For near-surface paths (region I), measuring all stress components is not feasible outside the laboratory. Even there, controlled strain-axis rotation must first be achieved. Meanwhile, hoop stress can be measured in situ; so can cylindrical radial motion and its principal stresses, in CIST-like events. To obtain the resulting stress-strain curves in the laboratory as well, is both the immediate reason for seeking improved sample-and-test procedures, and the proof that they work. Still, such proof, for which the curves in question are key (from CIST and surface-burst events), will not include rotation of axes unless a new way is found to measure stress in situ.

For region II, where all calculated paths are much simpler than on region I (through peak vertical displacement), it may be possible to limit in-situ stress-strain measurement to one event in each major type of geo-material. The first suitably-instrumented shot was fired in dry desert alluvium; its data (not yet available) extend from region II into region III. On strain paths in region IV, only hoop stress seems measurable [(ϵ_+, ϵ_-)-axes rotate, and strain is not plane], but even a subset of stress-strain curves puts a needed rein on models. Further, all stress-strain curves measured for in-situ material, either directly or by proven laboratory methods, become part of the strain-path model for that material. In addition, some of them form the data-base for mechanistic models - and predicting the rest is both the measure of such a model's value and a guide to its improvement. Laboratory stress-strain curves meet these needs about as well as curves measured on site; for, even if the two sets of curves differ appreciably, both apply

to real geo-substances (measurement error aside).

When a mechanistic model truly predicts the stresses measured along key strain paths, it then remains to measure its accuracy in predicting actual ground motion and stress in a surface-burst event. Thus, each such event is both a source of in-situ stress-strain curves and a gauge of model-accuracy. However, for the first one (in dry alluvium; above) the prior steps of laboratory measurement of stress on key strain paths, and evaluation/adjustment of models, were not taken. They should be carried out for future events, of which a surface burst now appears most cost-effective: Besides its twin uses (just noted) in developing models of such events, it can also help to validate models for contained, nearly spherical bursts, whose strain paths share basic properties with the paths of region II.

Much of this agenda is designed to boost knowledge of strain paths in surface bursts to a level already reached for contained, nearly spherical ones. At that level, generating new strain-path fields is secondary: For contained bursts, the main task is to fix the accuracy of ground-motion predictions made with models based on radial and hoop stresses measured in situ (and perhaps in the laboratory) along paths typical of Fig. 3. Clearly, such models bypass the questions of mechanism that dominate conventional modeling. Yet, success with strain-path methods will not obviate those questions. At a minimum, more insight into response mechanisms will permit more accurate interpolation among stress-strain curves, thereby reducing the number and cost of the curves needed for strain-path models. Also, though the set of curves required for free-field prediction is surprisingly small, it is clear (for surface-bursts at least; above) that models must have some power to extrapolate from the curves that are measurable. By design, strain-

path modeling reduces the need for such power; critical stress-strain curves are furnished by experiment. As a result, full advantage can be taken of mechanistic models, without letting their faults limit the reliability of ground-motion predictions.

Progress in modeling would be more rapid if complexity implied understanding. As it is, no two sites are identical, and the mechanistic models used to predict general ground motion are quilts whose every patch is intricate. Hence, while geo-materials are mechanically complex, we forgo knowledge of their dynamics when we try to apply all-purpose models to explosions in the earth, without showing that each mechanism in a given model really does affect key stress-strain curves as the model says. However difficult, such validation of each major model-element is the sine qua non of mechanistic modeling. Yet, for nearly spherical fields - and hence the source problem in nuclear monitoring - that task is of lower priority than strain-path modeling because:

i) The pertinent spherical strain-path fields are known and simple.

ii) It is practical - now - to measure stresses on those paths, both in situ and in the laboratory.

There is little reason and no need to press on with unvalidated models and postdiction. Headway will be made more surely, steadily and quickly by using already-adequate resources to create strain-path models - i.e., to a) measure stress in the laboratory on key strain paths, b) evaluate mechanistic models by comparing their stresses to those measured, c) modify a convenient mechanistic model, arbitrarily, so that it fits the measured stress-strain curves, d) measure stress and motion in situ, e) deduce in-situ stress-strain curves, and f) adjust sample-and-test procedures so that in-situ stresses are obtained in the laboratory. The accuracy

of the strain-path model [c)] is then found by comparing predicted and measured [d)] stresses and motions; so is the accuracy of the stress-strain curves given by current mechanistic models - a true overall test of their validity.

A pass or two through steps a)-f) will tell us, for any given medium, how accurately buried bursts can be defined as seismic sources, and how to predict them that well (three media predominate in nuclear monitoring). The process has begun for dry alluvium (a fourth medium), in which a buried 20-ton charge was fired. Step e) is now being taken with data from that shot, but sustained support is needed to see the cycle through step f) and final model-evaluation. Then, along with nuclear monitoring needs, the goals of several organizations can be served by repeating steps d) and e) for a near-surface burst. In addition, since a pregnant set of stress-strain curves is measured in steps a) and e), strain-path modeling is likely to prove an efficient way to learn about the mechanics of geo-materials - and whatever is learned will take a form of direct use to those concerned with explosively driven ground motion.

REFERENCES

Akers, S. (1983), 2nd and 3rd Quarterly Progress Reports for DNA Task Y99QAXSB, Work Unit 00019, U.S. Army Engineer Waterways Experiment Station, Vicksburg, MS.

ATI file; R. Hoy, H. Belchic, R. Miller, N. Short, R. Bendenelli and A. Mathews have independently confirmed that there was almost no water in Cowboy salt (1980). Their signed statements on the subject are on file at Applied Theory, Inc.

Bjork, R. (1972), "Computed Response of the Hudson Moon H.E. Experiment," Systems, Science and Software Topical Report No. 3SIR-976 (Contract DASA01-69-C-0165).

Bogart, J. and Schatz, J. (1983) "Specified Strain Path Testing of Geologic Materials," Rock Mechanics, Theory-Experiment-Practice: Proceedings of the 4th U.S. Symposium on Rock Mechanics Held at Texas A and M University June 20-23, 1983, C. Mathewson (ed), Texas A and M University, p.473.

Cherry, T. and Rimer, N. (1982), "Verification of the Effective Stress and Air Void Porosity Constitutive Models," VELA Seismological Center Topical Report No. VSC-TR-83-1, pp.6-15.

Heard, H., Abey, A., Bonner, B. and Duba, A. (1975), "Stress-Strain Behavior of Polycrystalline NaCl to 3.2 GPa," Lawrence Livermore Laboratory Report No. UCRL-51743.

Hoffman, H. and Sauer, F. (1969), "Operation Flint Lock, Shot Pile Driver, Project Officers Report - Project 1.1, Free Field and Surface Motions," Defense Atomic Support Agency Report No. POR-4000.

Ialongo, G. (1973), "Prediction Calculations for the Mixed Company Event III," Defense Nuclear Agency Topical Report No. DNA 30206T, pp.116-128 (Contract No. DNA001-72-C-0009).

Keogh, D., DeCarli, P. and Rosenberg, J. (1982), "Development of a High Modulus, Piezoresistive Gauge for Dynamic In Situ Soil Stress Measurements," Defense Nuclear Agency Report No. DNA-TR-82-17-V1.

Kitchens, C. (1972), "Numerical Experiments with the Compressible Navier-Stokes Equations," Proceedings of the International Conference on Numerical Methods in Fluid Mechanics, Vol I, H. Cabannes and R. Temam (eds), Springer-Verlag, p.120.

Ko, H-Y. (1981), "Cubical Test Data on Ralston Valley Soil," Systems Science and Software Report No. SSS-R-81-4824.

Lade, P. (1983), "Strain-Path Tests on Yuma Soil" (final report; Subcontract ATS-55-1; Contract No. DNA001-80-C-0232).

Murphey, B. (1960), "Particle Motions Near Explosions in Halite," Sandia Corporation Report No. SC-4440(RR).

Perret, W., Chabai, A., Reed, J. and Vortman, L. (1963), "Project Scooter," Sandia Laboratory Report No. SC-4602(RR), Chapter 4.

Perret, W. (1967), "Free-Field Particle Motion from a Nuclear Explosion in Salt, Part I," Report No. VUF-3012 (Vela Uniform Program).

Rimer, N. and Cherry, J. (1982), "Ground Motion Predictions for the Grand Saline Experiment," VELA Seismological Center Topical Report No. VSC-TR-82-25 (Contract No. F08606-79-C-0008), pp.23-25

Sauer, F. and Kochly, J. (1971), "Operation Diamond Dust, Project 3.1, Ground Motion Measurements," Defense Nuclear Agency Report No. POR 6437 (Contract No. DASA 01-69-C-0165).

Sauer, F. and Kochly, J. (1972), "Operation Diamond Mine, Ground Motion Measurements," Defense Nuclear Agency Report No. POR 6573 (final report; Contract No. DASA01-71-C-0014).

Seaman, L. (1974), "Lagrangian Analysis for Multiple Stress or Velocity Gauges in Attenuating Waves," J. Appl. Phys., p.4303.

Terhune, R. and Glenn, H. (1977), "Estimate of Earth Media Shear Strength at the Nevada Test Site," Lawrence Livermore Laboratory Report No. UCRL-52358, p.24.

Thomas, J. (1979), "Misers Bluff Negative Phase Measurements and a Pore-Air Model for Ground Motion Simulations," Proceedings of the Misers Bluff Phase II Results Symposium 27-29 March 1979, Volume I, Defense Nuclear Agency Report No. POR 7013-1, pp.3-181,182,183.

Tittman, B. (1983), "Studies of Absorption in Salt," Rockwell International Report No. SC5320.5FR (final report; Contract No. F49620-82-C-0015).

Trulio, J. and Perl, N. (1974), "Calculations in Support of the Diamond Dust and Diamond Mine Events," Defense Nuclear Agency Report DNA 3268F (Contract No. DASA01-69-C-0138).

Trulio, J., Ialongo, G., McDonald, J. and Srinivasa, D. (1975), "Overdrive Calculations Related to Nuclear Explosions," Defense Nuclear Agency Report No. DNA 3542F (final report; Contract DASA01-70-C-0074), Sections 4.2 and 8.

Trulio, J. (1975), "Stress Trajectory Analysis, Part I," Applied Theory, Inc. Report No. ATR-75-32-19(I) (Contract No. F04701-71-C-0016), Sections 1.2 and 3.1.

Trulio, J. (1977), "Ground Shock Deformation Fields," Report No. ATR-77-48-6 (final report; Contract No. F04704-76-C-0031), Section 2.

Trulio, J. (1978), "Simple Scaling and Nuclear Monitoring," Applied Theory, Inc. Report No. ATR-77-45-2 (final report on Phase IV of Contract No. DNA001-75-C-0304), p.22.

Trulio, J. (1981a), "Utility of Calculations" and "Strain Path Modeling," Proceedings of the Review of Free Field Ground Shock from Contained Nuclear Events, 8-9 Dec. 1981, R. Port (ed), R&D Associates, Marina del Rey, CA.

Trulio, J. (1981b), "Seismic-Wave Generation: Planning of In-Situ Experiments," Applied Theory, Inc. Report No. ATR-81-57-1 (Contract No. DNA001-80-C-0360), p.20.

Trulio, J. (1982), "Strain-Path Analysis and Testing, Proceedings of the Strategic Structures Review Conference, 4-6 May 1982, Vol. 1, Defense Nuclear Agency Internal Report No. DNA-IR-82-23-V1, p.267.

Trulio, J. and Port, R. (1982), "Material Properties for MX Land Basing," Applied Theory, Inc. Report No. ATR-55-82-1 (Contract No. DNA001-80-C-0232), Fig. 1.

Workman, J., Trulio, J. and Stokes, E. (1978), "Strain Fields Calculated from Measured Velocities: Axisymmetric Fields of Motion," Applied Theory, Inc. Report No. ATR-78-49-3 (final report; Contract No. F04704-75-C-0025), p.44.

Workman, J., Trulio, J. and Stokes, E. (1981), "Modeling the Behavior of Geologic Materials in Explosive Field Events," Air Force Weapons Laboratory Technical Report No. AFWL-TR-80-66 (final report; Contract No. F-29601-76-C-0015), pp.8-23.

Wright, J., Sandler, I. and Baron, M. (1973), "Ground Motion Calculations for Events II and III of the Middle Gust Series," Proceedings of the Mixed Company/Middle Gust Results Meeting 13-15 March 1973, Vol. II, Defense Nuclear Agency Report No. DNA 3151P2, pp.638 and 639.

APPENDIX

At first, equations for elastic-plastic behavior were added to those previously developed for hydrodynamic motion. The constitutive models then featured i) general (nonlinear) elastic hydrostats and a linear elastic description of shear, giving way to ii) plastic flow at prescribed limits of shear strength, in accord with one flow rule or another. Also, iii) transitions between condensed and gaseous states were made hydrostatically; to deal with porous solids, iv) the hydrostats were further generalized to encompass inelastic volume changes during compression ("compaction").

Elements i)-iv) still form the backbone of computational models of explosively driven earth motion. However, a major conceptual step was taken by requiring that the stress-strain relations for compaction, shear failure and elastic deformation conform to Drucker's postulates. Equations for those three modes of deformation, which had been stitched together largely on an ad hoc basis, then form a single, internally consistent set. Yield surfaces expressing the limits of material strength in shear and compression, occupy a central place in that set. By allowing yield surfaces to vary during shear failure, inelastic strains can be held to realistic levels for frictional materials - a major reason for moving to Drucker's postulates. Though a part of the apparatus for describing inelastic deformation (of which flow rules are another part), the growth and shrinkage of yield surfaces ("hardening" and "softening") make possible such wide variations in material behavior as to form a fifth basic element of the models (element v)).

Both yield surfaces and hydrostats are affected by shock heating. Those effects are usually small (shocks from bursts decay rapidly as they travel), but are included in the models (element vi)). With regard to hydrostats, the laws of thermodynamics provide a basis for so doing, whereas estimates of thermal effects on strength have largely been guesses.

Other processes are now described by the models in ways that lie outside the framework of Drucker's postulates. Prominent among them is tensile failure, as distinct from cracking in shear (element vii)). Present models of tensile failure include equations for crack nucleation and spreading, and also for the changes in strength and moduli that attend crack damage. Those equations are ancillary to the rest of the model (elements i)-vi)). So are equations for multiphase flow, of which there are at least three major sets: viii.a) pore-air equations, describing the flow of air into or out of the ground, where it interacts thermomechanically with particles of earth; viii.b) equations for the diffusion of water through networks of cracks in rocks, with attendant thermomechanical effects; ix) equations for the sweep-up of dust and debris from the ground surface by burst-induced winds.

The development and use of models incorporating all these elements was well under way ten years ago. It has since been made clear that soils, at least, can depart from the normality condition to which Drucker's postulates lead (when taken with certain other assumptions). Hence, modelers are now free not only to employ yield surfaces that vary widely in any given material element, but to relate increments of stress and inelastic strain in ways that are independent of their variable yield surfaces. In short, the flow rule has become a tenth model-element (element x)). More recent is element xi) - "subsidence" - a relative of the shock-damage idea; in this case a shock breaks down a lightly cemented matrix of saturated granular material, and the resulting particles settle (under gravity) to a relatively well-packed state - leaving a relatively large crater. Many current models also describe rate effects (element xii)), for which we note here only the vast range of modeling possibilities they open: a) Stress increments become linear combinations of both the incremental strain and strain-rate tensors (though the usual constitutive

tensor may "simply" become a function of strain rate if causality is strictly enforced), and b) both the flow rule itself (element x)) and the hardening/softening yield surface become functions of strain rate. Another fairly recent part of models is tectonic energy release (element xiii)); an older part provides for orthotropy in layered media (element xiv)). Moreover, when media are heterogeneous, site structure allows some freedom of model-variation; that structure, never exactly known, has to be idealized.

Rarely are all these elements used in one calculation, but most of them often are - and the complexity of the individual elements has hardly been hinted at. As a small example, nonlinear elasticity calls for a) definition of strain energy as a function of at least the three strain invariants, b) knowledge of how yielding (Bjork 1972, p.5,6) and cracking affect that function, and c) its integration into models that include heating and rate effects. Each of these items is dealt with in full by all models, but mainly by default: The many material-specific functions they entail are almost unknown for geo-materials - as is the cumulative effect of myriad decisions (and non-decisions) modelers make about such items when a specific geo-material is modeled.

DISTRIBUTION LIST

DEPARTMENT OF DEFENSE

Assistant to the Secy of Defense, Atomic Energy
ATTN: Executive Asst

Defense Nuclear Agency
ATTN: SPTD
4 cy ATTN: STTI/CA
2 cy ATTN: SPSS

Defense Tech Info Ctr
12 cy ATTN: DD

Field Command/DNA, Det 1
Lawrence Livermore National Lab
ATTN: FC-1

Field Command, Defense Nuclear Agency
ATTN: FCPR
ATTN: FCT
ATTN: FCTT
ATTN: FCTXE
ATTN: FCTT, W. Summa

Under Secy of Def for Rsch & Engrg
ATTN: Strat & Space Sys (OSO)

DEPARTMENT OF THE ARMY

Harry Diamond Laboratories
ATTN: DELHD-NW-P, 20240
ATTN: 00100 Commander/Tech Dir/Div Dir

US Army Ballistic Research Labs
ATTN: DRDAR-BLT, J. Keefer
ATTN: DRDAR-BLA-S, Tech Lib

US Army Chemical School
ATTN: ATZN-CM-CS

US Army Cold Region Res Engr Lab
ATTN: CRREL-EM

US Army Engr Waterways Exper Station
ATTN: Library
ATTN: WESSA, W. Flathau
ATTN: F. Hanes
ATTN: J. Ingram
ATTN: WESSE, D. Day

US Army Material Command
ATTN: DRXAM-TL, Tech Lib

US Army Nuclear & Chemical Agency
ATTN: Library

US Army White Sands Missile Range
ATTN: STEWS-TE-N, K. Cummings

DEPARTMENT OF THE NAVY

David Taylor Naval Ship R&D Ctr
ATTN: Code L42-3, Library
ATTN: Code 1770

Naval Surface Weapons Ctr
ATTN: Code F31

DEPARTMENT OF THE AIR FORCE

AF/INT
ATTN: INT

Air Force Institute of Technology
ATTN: Library

Air Force Weapons Laboratory
ATTN: NTE, M. Plamondon
ATTN: DEX, J. Renick
ATTN: SUL
ATTN: DEX

Air University Library
ATTN: AUL-LSE

Ballistic Missile Office/DAA
ATTN: PP
2 cy ATTN: ENSN

Strategic Air Command
ATTN: DOM

DEPARTMENT OF ENERGY

Department of Energy
Albuquerque Operations Office
ATTN: CTID

Department of Energy
Nevada Operations Office
ATTN: Doc Con for Tech Library

OTHER GOVERNMENT AGENCIES

Central Intelligence Agency
ATTN: OSWR/NED

Department of the Interior
ATTN: D. Roddy

Federal Emergency Management Agency
ATTN: Ofc of Rsch/NP, D. Bensen

NATO

NATO School (SHAPE)
ATTN: US Documents Officer

DEPARTMENT OF ENERGY CONTRACTORS

University of California
Lawrence Livermore National Lab
ATTN: Tech Info Dept Library

Los Alamos National Lab
ATTN: J. Hopkins

Oak Ridge National Laboratory
ATTN: Civ Def Res Proj, Mr. Kearny

Sandia National Laboratories
ATTN: L. Vortman
ATTN: Tech Lib 3141
ATTN: A. Chaban

DEPARTMENT OF ENERGY CONTRACTORS (Continued)

Sandia National Laboratories
ATTN: Library & Security Class Div

DEPARTMENT OF DEFENSE CONTRACTORS

Acurex Corp
ATTN: K. Triebes

Aerospace Corp
ATTN: Library Acquisition M1/199

Agbabian Associates
ATTN: M. Agbabian

Applied Research Associates, Inc
ATTN: R. Frank

Applied Research Associates, Inc
ATTN: D. Piepenburg

ARTEC Associates, Inc
ATTN: D. Baum

Applied Theory, Inc
2 cy ATTN: J. Trulio

BDM Corp
ATTN: Corporate Lib
ATTN: T. Neighbors

Boeing Co
ATTN: Aerospace Library

California Research & Technology, Inc
ATTN: K. Kreyenhagen

California Research & Technology, Inc
ATTN: F. Sauer

Cushing Associates
ATTN: V. Cushing

Develco, Inc
ATTN: L. Rorden

EG&G Wash Analytical Svcs Ctr, Inc
ATTN: Library

Electro-Mech Systems, Inc
ATTN: R. Shunk
ATTN: H. Piper

General Research Corp
ATTN: R. Parisse
ATTN: E. Steele

Geo Centers, Inc
ATTN: L. Isaacson
ATTN: H. Linnerud

H-Tech Labs, Inc
ATTN: B. Hartenbaum

Horizons Technology, Inc
ATTN: R. Kruger

IIT Research Institute
ATTN: Documents Library

DEPARTMENT OF DEFENSE CONTRACTORS (Continued

Kaman Sciences Corp
ATTN: Library

Kaman Tempo
ATTN: DASIAC
ATTN: J. Shoutens

Kaman Tempo
ATTN: DASIAC

Merritt CASES, Inc
ATTN: J. Merritt
ATTN: Library

Mitre Corp
ATTN: J. Freedman

University of New Mexico
ATTN: N. Baum

Pacific-Sierra Research Corp
ATTN: H. Brode, Chairman SAGE

Physics Applications, Inc
ATTN: C. Vincent

Physics International Co
ATTN: Tech Lib

R&D Associates
ATTN: G. Ganong

R&D Associates
ATTN: J. Lewis
ATTN: Technical Info Ctr
ATTN: P. Haas

Rand Corp
ATTN: B. Bennett

Rand Corp
ATTN: P. Davis

S-CUBED
ATTN: D. Grine
ATTN: Library

Science & Engineering Associates, Inc
ATTN: H. Linnerud

Science & Engrg Associates, Inc
ATTN: J. Stockton
ATTN: B. Chambers III

Science Applications Intl Corp
ATTN: K. Sites

Science Applications Intl Corp
ATTN: W. Layson

Science Applications, Inc
ATTN: Technical Library

Southwest Research Institute
ATTN: A. Wenzel
ATTN: W. Baker

Structural Mechanics Associates, Inc
ATTN: R. Kennedy

DEPARTMENT OF DEFENSE CONTRACTORS (Continued)

SRI International
ATTN: P. De Carli
ATTN: D. Keough
ATTN: G. Abrahamson

Teledyne Brown Engineering
ATTN: F. Leopard
ATTN: D. Ormond

Terra Tek, Inc
ATTN: S. Green

Weidlinger Assoc, Consulting Engrg
ATTN: T. Deevy

DEPARTMENT OF DEFENSE CONTRACTORS (Continued)

TRW Electronics & Defense Sector
ATTN: Technical Info Ctr
2 cy ATTN: N. Lipner

TRW Electronics & Defense Sector
ATTN: E. Wong
ATTN: P. Dai

Weidlinger Assoc, Consulting Engrg
ATTN: J. Isenberg

Weidlinger Assoc, Consulting Engrg
ATTN: M. Baron

END

FILMED

6-85

DTIC